Highly selective conversion of mixed polyolefins to valuable base chemicals using phosphorus-modified and steam-treated mesoporous HZSM-5 zeolite with minimal carbon footprint

Andreas Eschenbacher [a], Robin John Varghese [a], Evangelos Delikonstantis [b], Oleksii Mynko [a], Farnoosh Goodarzi [c], Kasper Enemark-Rasmussen [c], Jogchum Oenema [a], Mehrdad Seifali Abbas-Abadi [a], Georgios D. Stefanidis [a,d], Kevin M. Van Geem [a,*]

[a] *Laboratory for Chemical Technology (LCT), Department of Materials, Textiles and Chemical Engineering, Faculty of Engineering & Architecture, Ghent University, Technologiepark 125, 9052 Zwijnaarde, Belgium*
[b] *AristEng S.à r.l., 77, Rue de Merl, L-2146 Luxembourg City, Luxembourg*
[c] *DTU Chemistry, Technical University of Denmark, Kemitorvet Building 207, 2800 Kgs. Lyngby, Denmark*
[d] *School of Chemical Engineering, National Technical University of Athens, Iroon Polytechniou 9, Athens 15780, Greece*

ARTICLE INFO

ABSTRACT

Catalytic fast pyrolysis of polyolefinic waste streams was investigated to recover valuable base chemicals at high selectivity. HZSM-5 zeolite with different properties, affected by Si/Al, mesoporosity, phosphorus stabilization, and steaming, were tested and thoroughly characterized. Different feeds, catalyst/feed ratios and reaction temperatures were evaluated in a micropyrolysis reactor coupled to two-dimensional gas chromatography. While unmodified HZSM-5 rapidly deactivated, phosphorus-modified and steamtreated HZSM-5 showed almost no deactivation due to its lower coking propensity during 130 runs with stable conversion towards C_{5+} aliphatics and high C_2-C_4 olefins selectivity (~75%) using post-consumer mixed polyolefins. The performance of this direct olefins production route with unprecedented high olefin selectivity was further evaluated in a plantwide context. It was found that it requires ~37% lower energy input than the plastics pyrolysis followed by pyrolytic oil steam cracking, while it results to at least a one order of magnitude lower environmental burden as compared to waste incineration.

1. Introduction

Olefins (i.e., ethylene, propylene, and butenes) and aromatics (i.e., benzene, toluene, and xylenes) are key building blocks in the production processes of many materials used in our daily lives. For the production of thermoplastics (PE, PP, PET, PS, etc.), the International Energy Agency forecasted an increased production of roughly 600 Mt of thermoplastics in 2050, double the production level of 2010 [1]. To support this increasing production of plastics, also the demand for the above-mentioned base chemicals continues to grow [2]. To date, these are primarily produced from fossil resources via steam cracking and to a lesser extent as a by-product from fluid catalytic cracking [3–6].

Producing plastics from fossil recourses has a high carbon footprint due to the energy-intensive production processes. In addition, polyolefins are challenging to recycle mechanically since the end-of-life mixed polyolefins waste is often contaminated with other plastics (PET, PS, PU, PA, …) and inorganics such as metals from pigments, fillers, or dirt [7–10]. Besides being "downcycled" by mechanical recycling to lower value products, their energy content is often valorized by incineration, leading to further fossil-based CO_2 emissions [11]. Chemical recycling via pyrolysis and steamcracking is seen as a promising technology for the recycling of polyolefins to produce new plastics with identical properties to virgin, fossil-derived plastics. This route involves the pyrolysis of sorted plastic yielding ~80–90% transportable liquid with a

broad carbon number distribution, ranging from C_1 to heavy waxes having different structures [12,13], ii) decontamination of the liquid to very low contaminant levels [14,15], and iii) steam cracking with a ~70% efficiency to monomers, i.e., C_2-C_4 olefins and monoaromatics [11]. While carbon losses to coke are moderate (~0.5 wt%) during steam cracking, the high furnace temperature of ~850 °C renders steam cracking energy intensive and the high production of fuel gas (15–25% [11,16]), which is combusted to provide the heat for operation, results in high CO_2 emissions. Furthermore, at current crude oil prices (app. $70/bbl, 07–2021) this approach is more expensive than directly using fossil feeds and requires intensive processing to remove contaminants. To date, with less than < 1% being recycled back to monomers [17], there is a clear demand for more efficient monomer recovery development. Within this work, the direct upgrading of polyolefin pyrolysis vapors over a catalyst in the vapor phase was studied using modified H-ZSM-5 zeolites. This integrated process comprises fewer steps compared to the incumbent approach of pyrolysis, liquid product de-contamination, and steam cracking, while the use of a catalyst allows to operate at lower temperatures, which is expected to benefit process efficiency [18–22]. By physically separating the pyrolysis and the close-coupled catalytic upgrading e, the direct contact of non-volatile inorganic contaminants with the catalyst was avoided. This can prevent the poisoning of acid sites, as was reported when processing ash-containing biomass in direct catalyst contact [22–25].

In the present work, HZSM-5 with high to medium Al density was studied (Si/Al of 15–23) and mesopores were incorporated via a desilication procedure [26–28], thereby creating hierarchical zeolites with both micro-and mesoporosity. Since the mesopores are connected to the micropores and the external surface of the crystallites, the micropore diffusion pathway of reactants/products is shortened, thereby limiting undesired secondary reactions [29–32]. For the proposed conversion of polyolefin-derived pyrolysis vapors, which are ~70% C_{21+} of linear hydrocarbons waxes, this may allow to improve the selectivity to olefins since longer residence time within zeolite micropores increases the probability of additional encounters with acid sites that can lead to secondary reactions such as Diels-Alder, polymerization and coke formation of the highly reactive olefins. Depending on the composition (molecular weight) of the vapors, diffusion into micropores might be hampered and for cracking of heavy feed or naphtha, increased light olefin yields were reported after introducing mesoporosity to HZSM-5 [3,33]. This was explained by increased accessibility of bulky molecules, which may then, after pre-cracking at acid sites located externally or in the mesopores, diffuse further into the micropores and react towards smaller products. Even after steaming the mesoporous and conventional HZSM-5, the mesoporous version resulted in a higher yield of light olefins [3]. A third benefit of incorporating mesopores may be that when coke builds up over time under continuous operation, mesoporous HZSM-5 tends to deactivate slower than its non-mesoporous counterpart does. This aspect was shown for highly aromatic and oxygenated feeds [28,34–36] but has to the best of our knowledge not yet been investigated for upgrading of polyolefin-derived pyrolysis vapors.

The hydrothermal stability of HZSM-5 can be improved by the addition of phosphorus [37–47]. While the phosphorus introduction initially decreases the acidity compared to the non-treated HZSM-5 [41], the phosphorus-modified HZSM-5 retains its acid sites to a higher level after high severity steaming compared to the untreated zeolite due to improved stability of framework aluminum species against dealumination [40,46–49]. Phosphorus loadings of ~1.5–2 wt% were reported favourable for maximum retention of strong acid sites after steam treatment of HZSM-5 with Si/Al ratios of 25–40 [37,40,50]. Advantageously, the phosphorus modification also improves the selectivity towards light olefins [37], and maximum selectivities for propylene during alkene cracking were reported with weight loadings of ~2 wt% [51–53], while higher loadings of ~3 wt% led to a clear drop in propylene selectivity, e.g., for C_4 olefin cracking the propylene yield increased from 35 to 43 wt% using steamed versions of parent HZSM-5 and

HZSM-5 modified with 1.8 wt% P, but it decreased to 31 wt% when the P loading was 2.8 wt% [51]. Similarly, for the cracking of *n*-hexane, *n*-decane, and naphtha, optimum P/Al ratios in the range of 0.4–0.7 were reported for optimum activity and hydrothermal stability, while higher phosphorus loadings led to lower conversions due to reduced accessibility [37,40,54]. The steam treatment of the phosphorus-modified HZSM-5 can further improve the selectivity to light olefins, e.g., for butene cracking at 530 °C the propylene yield of HZSM-5 (Si/Al ~35) modified with 1.7 wt% P was 38% and it improved to 43% after steaming the catalyst at 800 °C [51]. Since steam treatment lowers the acidity of the catalyst, it can also reduce the coking propensity, and steamed P-modified HZSM-5 showed a lower rate of coke formation than the parent HZSM-5 for *n*-hexane cracking [39] Another motivation for steam-treating a catalyst are scale-up considerations. The activity remaining in the zeolite that was steamed under high-severity at 800 °C can be regarded stable under the hydrothermal conditions present during reaction and regeneration conditions, which are not expected to exceed 700 °C in catalytic plastic cracking processes. Therefore, yields obtained with a steamed catalyst present a more valuable estimate for the catalyst's long-term productivity and selectivity while yields obtained with a fresh catalyst would inevitably change over time due to dealumination.

In this study, for the first time, we attempted to harness the benefits of mesoporosity, phosphorus modification, and steam treatment of HZSM-5 zeolites to maximize the recovery of C_2-C_4 olefins from polyolefins via catalytic upgrading of pyrolysis vapors. The use of two-dimensional gas chromatography provided detailed quantitative product distribution using different virgin polyolefin types and post-consumer mixed polyolefin (MPO), different catalysts, and different operating conditions (temperature, catalyst/feed ratio). Lastly, also the catalytic activity of a selection of the best performing catalyst during repeated reaction/regeneration cycles, and the change in product distribution was studied. Furthermore, the catalyst performance was evaluated in a plantwide context, focusing on the energy and carbon footprints of such a catalytic process. The results were benchmarked against other peer processes to highlight the significance of the current catalyst impact. The combination of these different aspects shows the enormous potential for industrial applications of the proposed route.

2. Methodology

2.1. Feedstock

Virgin LDPE and LLDPE were purchased from ExxonMobil (LDPE LD 150 Series and Exceed™ 1012HA), HDPE was obtained from Dow (HDPE 25055E), and PP was provided by Borealis (HE125MO). The as-received pellets were downsized using a cutting mill (FRITSCH). The obtained powder was sieved to obtain a fraction with particle size < 300 μm, which was used for the micropyrolysis tests to avoid mass and heat-transfer limitations.

The post-consumer mixed polyolefinic waste (MPO) was prepared by cold-washing of sorted polyolefinic waste, with an approximate composition of 75 wt% PE, 16 wt% PP and 9 wt% rest. The rest fraction roughly consists of ~2% PA, ~1% PET, ~1% PS, and ~5% non-polymers such as metals/inorganics and paper/wood/food residue not sufficiently removed by the cold-washing and pelletization process. The cold-washed flakes were extruded with 400 μm screens and high temperatures (290 °C) into pellets. For the pyrolysis tests, the pellets were downsized using a CryoMill to obtain particles < 300 μm. While virgin polyolefins comprise ~100% volatiles when heated [55], MPO was composed of 96.9% volatiles, 0.3 wt% fixed carbon, and 2.8 wt% ash [56]. The elemental content of the different feeds was determined using a Thermo Scientific FLASH 2000 analyzer, with more details provided in prior work [56]. Based on its molecular formula, the elemental composition of the high purity virgin polyolefins is calculated to 85.7% C and 14.3% H, whereas the elemental composition of MPO was

determined to 83.7% C, 14.2% H, 0.35% N, and 1.7% O on an ash-free basis [56].

2.2. Catalyst preparation

As parent material, HZSM-5 with nominal SiO_2/Al_2O_3 ratio of 30 and 55 were obtained from Zeolyst International (sample code CBV 3024E and CBV 5524 G), and transformed from the as-received ammonium from to the proton form via calcination in dry air flow at 550 °C for 5 h. These parent HZSM-5 are abbreviated with *Z30* and *Z55* in the following. Mesopores were introduced into parent HZSM-5 via desilication with NaOH solution followed by mild acid wash, as outlined in earlier work [28], generating *mesoZ30* and *mesoZ55*.

The desired content of phosphorus was added to *mesoZ30, mesoZ55*, and *Z55* using H_3PO_4 as the precursor. The desired amount of 85 wt% H_3PO_4 (Merck) was diluted with purified water to prepare a solution 10 times the zeolite weight. Zeolite and H_3PO_4 solution were then mixed and stirred for 2 h at room temperature. In a rotary evaporator, the water was slowly evaporated during ~1 h from the suspension at 75 °C while lowering the pressure to 100 mbar. Then, the residue was dried at 120 °C overnight and calcined in a flow of synthetic air by ramping the temperature to 550 °C during 4 h and holding the final temperature for 4 h, producing samples *P/mesoZ30*, *P/mesoZ55*, and *P/Z55*.

For the steam treatment of *P/mesoZ30*, *P/mesoZ55*, and *P/Z55*, the different zeolite samples (~2 g) were pelletized to obtain particles > 500 μm and loaded in a quartz tube (ID = 23 mm, length 850 mm) supported in between plugs of quartz wool. The quartz tube was placed inside a vertical furnace with three controlled heating zones. The temperature of the catalyst was monitored with two thermocouples measuring inside the quartz tube at the start and end of the fixed bed. N_2 was used as carrier gas at 30 g/h. After gradually increasing the temperature of the furnace to reach a catalyst temperature of 500 °C (mild steaming, suffix "ms") or 800 °C (severe steaming, suffix "ss"), steaming was initiated by feeding deionized H_2O at 350 g/h into a preheater operated at 350 °C, thus generating a stream with 95 vol% steam introduced to the reactor. The steam treatment lasted for 300 min under mild conditions and 240 min for the severe conditions while maintaining the catalyst temperature at the setpoint ± 10 °C. After steaming, the samples *P/mesoZ30-ms*, *P/mesoZ30-ss, P/mesoZ55-ss*, and *P/Z55-ss* were obtained. Since in the course of the investigation it was found that a high aromatization activity remained for *P/mesoZ30-ms* after the mild steaming (see Results section), the need for a severe steaming treatment became apparent and no mildly steamed versions of *P/mesoZ55* and *P/ Z55* were prepared and tested.

2.3. Catalyst characterization

The PXRD patterns were measured with a Bruker D8 Advance powder diffractometer in reflection mode using Cu Kα1 (λ = 1.5406 Å) radiation. The diffractograms were measured between 3 and 90 degrees 2θ and 0.038 step size. Details on the N_2 physisorption [57] and Ar physisorption were reported in earlier work [28]. Imaging of zeolite particles with transmission electron microscopy (TEM) was achieved using a Tecnai T20 G2 (acceleration voltage of 200 kV) [28]. The content of Si, Al, and P content of the tested zeolites was analyzed according to the methodology described in prior work utilizing XRF [23]. The acidity of the catalysts tested in this work was analyzed by NH_3-TPD using an AutoChemII instrument (Micromeritics) as described in more detail in the supporting information. Fourier Transform Infrared (FTIR) spectra were recorded in transmission mode on a Bruker Tensor 27 instrument equipped with an MCT detector, using 32 scans per spectrum and a resolution of 4 cm^{-1}. Samples were pressed into self-supporting pellets of ~12 mg using a pellet die (ID = 13 mm) and placed into an vacuum cell equipped with CaF_2 windows. Next, the samples were dried under active vacuum (p < 10^{-5} mbar) up to 550 °C (10 °C/min) and held at that temperature for 1 h. After drying, the cell was cooled down to

150 °C and a spectrum was measured. Pyridine (redistilled, 99.9%, Sigma- Aldrich) was introduced into the cell as vapor at a pressure of ~14 mbar, and was adsorbed for 30 min subsequent by 30 min of evacuation whereafter a spectrum was measured of the adsorbed pyridine. For quantification of the number of acid sites, the spectrum of the dehydrated sample was subtracted from the spectrum obtained after 30 min of evacuation to obtain a difference spectrum. The absorption bands at 1453 cm^{-1} and 1545 cm^{-1} corresponding to pyridine adsorbed on Lewis and Brønsted acid sites, respectively, were integrated and corrected for pellet mass and their apparent integral absorption coefficients (2.22 cm•μmol^{-1} for Lewis acid sites and 1.67 cm•μmol^{-1} Brønsted acid sites) to obtain the number of acid sites [58].

All solid-state NMR spectra were recorded on a Bruker AVANCE III HD spectrometer operating at a magnetic field of 14.05 T equipped with a 4 mm CP/MAS BBFO probe. ^{27}Al MAS NMR spectra were acquired with the one-pulse experiment using a 0.5 μs π/6 excitation pulse and an interscan delay of 0.5 s ^{29}Si MAS NMR spectra were acquired using a 4.75 μs π/2 pulse and an interscan delay of 60 s ^{31}P MAS NMR spectra were acquired using a 2.9 μs π/2 pulse and an interscan delay of 60 s The spinning frequency was 7 kHz for all spectra. High-power ^{1}H decoupling was employed during acquisition of all spectra. All ^{27}Al, ^{29}Si and ^{31}P chemical shifts are reported relative to aqueous $Al(H_2O)_6^{3+}$, TMS, and 85% H_3PO_4 at 0 ppm, respectively.

2.4. Micro-pyrolyzer and product analysis

The experiments were carried out using a single-shot tandem micropyrolysis system (Rx-3050TR, Frontier Labs, Japan) coupled to two-dimensional gas chromatography (GC) and a separate GC dedicated for the analysis of light gases. 60 mL/min of He was used as the carrier gas in the micropyrolyzer, resulting in a catalyst contact time of ~80 ms, while at the point of reaction, the pressure of the GC inlet and inside the reactors was ~2.7 bara. The column flow was set to 2.1 mL/min. For the present work, the pyrolysis reactor was operated consistently at 550 °C, since pyrolysis temperatures of 500 °C or lower lead to significantly broader volatilization profiles [56]. For each reaction, 0.4 ± 0.02 mg of ground material was loaded into a deactivated stainless steel sample cup (Eco-cup SF) using a high precision balance and then dropped into the preheated pyrolysis furnace. Helium as carrier gas purged the volatiles into the second reactor, which contained a quartz tube loaded with the catalyst fixed bed. The catalyst was secured between two quartz wool plugs and placed inside the temperature-controlled isothermal zone of the upgrading reactor (see Fig. S1), for which different temperatures between 500 and 700 °C were studied in the present work. The catalyst (100–300 μm particle size) was diluted in highly inert α-Al_2O_3 with a low surface area of 0.04 m^2/g. The dilution of the catalyst prevented channeling or bypass flow and maintained similar bed lengths across different catalyst loadings and catalyst densities [34].

The products exiting the upgrading reactor entered the GC × GC oven and were firstly trapped in a column section cooled with liquid nitrogen for 5 min while the GC oven was held at − 40 °C by cryogenic cooling. Then, the cryo-trap was switched off and trapped vapors were released in a refocused manner according to their boiling points while heating the oven at 3 °C/min to 320 °C. Prior to entering the GC × GC separation, the column flow was branched to reach a customized multicolumn GC (Trace 1300) for light gas analysis. For the GC × GC separation, a two-stage cryogenic modulator (liquid CO_2) was positioned between the first and second dimension column (modulation time 5 s). The 1st dimension column was a non-polar RTX-1 PONA (50 m, ID = 0.25 mm) and the 2nd dimension column was a polar BPX-5 column (2 m, ID = 0.15 mm).

The effluent from GC × GC separation was analyzed by FID for product quantification. The FID response was determined by dosing different amounts of iso-butane (5%, balance He). For product identification, a BenchTOF-Select™ (Markes, United Kingdom) was used, scanning in a range of m/z = 20–600 at 70 eV. MS spectra were

compared with the NIST library database (MS search 2.2). Data processing was performed using GC Image software, and the yields of products were calculated using the effective carbon number approach [59].

The cryogenic trap did not trap light gases such as methane, ethylene, and propylene. These three peaks could be well separated and quantified using the FID detector. Once the cryotrap was switched off, initially the C_4 components (1-butene, 1,3-butadiene, n-butane, and 2-butenes) eluted from the column and this was followed by the elution of well-separated C_{5+} products. It is noted that any ethane and propane in the products would co-elute with ethylene and propylene. However, the yields of ethane and propane are deemed fairly low and therefore only a small error and overestimation of the ethylene and propylene yields is made. This is supported by several aspects. Firstly, the MS identification of the product peaks showed a clear match with ethylene and propylene. Secondly, the yield of C_1 and C_4 alkanes was low (<1 wt %), indicative of a low extent of "overcracking" and hydrogen transfer due to the short vapor residence times and moderate upgrading temperatures. Therefore, also the yield of ethane and propane can be expected to be minor. This is supported by results reported by other researchers using a similar micropyrolyzer as used in the present work and ex-situ catalytic upgrading of PE vapors over a HZSM-5 catalyst, as these researchers reported a C_2, C_3, and C_4 olefinicity (=weight fraction of olefins) of only 4%, 6%, and 3%, respectively [60]. Yields are reported in wt% of feed, whereby the feed is inorganics-free. This is already the case for virgin plastics, but for MPO, the feed contained an appreciable amount of 2.8 wt% inorganics [56], and yields are therefore reported based on the organic fraction of the feed. For simplicity, normalizing the product yields determined by FID did not consider coke on the catalyst, or minor amounts of hetero-atom containing light gases such as CO/CO_2. These combined losses to coke and heteroatom-containing light gases amount to less than 5%. As an example, a reported yield of 80 wt% C_2-C_4 olefins from normalizing may then, in reality, correspond to only 76 wt%, if there would be a high coke yield and all heteroatoms would be released as gases (not quantified). However, this is a conservative estimation since the highest coke yields in the present work were in ~1 wt%; thus, in fact less than 5% relative error results by normalizing without taking coke and hetero-atom containing light gases into account. The repeatability of the product analysis was confirmed by randomized repetitions of selected tests throughout the test series. In addition, the repeatability of the product analysis is illustrated based on the results obtained from six reaction/regeneration cycles that yielded nearly identical product distribution, and the uncertainty assessment from these repetitions is summarized in Table S1.

Within this work the product yields are presented for CH_4, ethylene, propylene, 1,3-butadiene, and other C_4 olefins (C_4 =), C_4 alkanes, aromatics, the aromatic-free C_5-C_{11} fraction, C_{12}-C_{20} hydrocarbons, and C_{21}-C_{35} hydrocarbons. The grouping of the C_{5+} products facilitates the interpretation of the results as the focus of the present work lies on the production of light (C_2-C_4) olefins. For selected individual tests, the complete yield structure involving all detected compounds detected by GC × GC/FID is disclosed in Table S7.

Coke deposits on the catalyst were quantified after several runs without regenerating the catalyst by oxidation using an elemental analyzer or TGA.

3. Results

3.1. Catalyst properties

Table 1 summarizes the physicochemical properties of the studied catalysts. Compared to the parent *Z30* and *Z55,* the *P/mesoZ30-ss* and *P/mesoZ55-ss* had increased mesoporosity. The mesoporosity was even higher for *mesoZ30* and *mesoZ55* before their phosphorous modification and steaming [28], but had decreased by ~0.05 cc/g for *P/mesoZ30-ss* and *P/mesoZ55-ss* (Table 1). The presence of mesopores was visualized using bright-field TEM (Fig. 1, Fig. S2). Mesopores appear well distributed throughout the zeolite particles for *P/mesoZ30* (Fig. S2a+b) but appear less homogenously distributed for *P/mesoZ55*, with sometimes larger mesopores observed in the center of the zeolite particles (Fig. S2c+d). This could have been the result of Al-zoning in the commercial samples [61–63], with a more Al-rich rim that was less prone to desilication. Considering the high level of mesoporosity developed in *P/mesoZ30,* it is possible that the increased steaming severity at 800 °C caused a partial collapse of the structure, leading to a decrease in mesoporous volume compared to the mildly steamed version (Table 1). Further, it is noted that after P-modification and steaming, the micropore volume had decreased from 0.13 cc/g to 0.07 cc/g, as determined by N_2 physisorption (Fig. S3) using the *t-plot* method. This is attributed to the deposition of P inside the micropores, blocking of pore-openings by extra-framework Al created by the phosphorus impregnation, and steaming [40].

Prior to steaming, *mesoZ30* already had a lower crystallinity (from XRD analysis) compared to m*esoZ55* since more harsh conditions were required to achieve desilication of *Z30* compared to *Z55* [28], and increased concentrations of NaOH solutions used in the desilication result in decreased crystallinity [64,65]. The steam treatment did not lead to a marked decrease in crystallinity (see Fig. 1 and Fig. S4), with *P/mesoZ30-ss* and *P/mesoZ55-ss* showing 1% and 2% lower crystallinity than *P/mesoZ30* and *P/mesoZ55* according to the integrated peak areas in the range of 22.5–25.0° 2θ (ASTM D 5758 – 01). Generally, the crystallinity is not affected by steaming at moderate temperatures of

Table 1
Physicochemical properties of phosphorus modified and steam- catalysts in comparison unmodified parent versions. "ms" and "ss" in suffix corresponds to mild and severe steaming.

	Z30	*P/mesoZ30-ms*	*P/mesoZ30-ss*	*Z55*	*P/Z55-ss*	*P/mesoZ55-ss*
V_{micro}[a] [cc/g]	0.21	0.09	0.06	0.22	0.06	0.17
V_{micro}o[b] [cc/g]	0.13	0.10	0.07	0.13	0.07	0.07
V_{meso}[c] [cc/g]	0.08	0.09	0.12	0.09	0.06	0.11
V_{total}[d] at p/p$_0$ = 0.99	0.35	0.27	0.32	0.31	0.30	0.43
BET area[d] [m^2/g]	416	352	357	423	401	349
Acidity[e] [mmol NH$_3$/g]	0.88	0.48	0.15	0.65	0.10	0.09
Si/Al[f]	16.4	13.0	13.0	28.5	28.8	19.2
Framework Si/Al[e]	n.d.	n.d.	50	55.6	84	85
P/Al	–	0.6	0.6	–	1.2	0.6
P loading (wt%)	–	2.0	2.0	–	1.9	1.4
Brønsted acid sites (mmol•g^{-1})[g]	0.26	0.08	0.03	0.26	0.05	0.02
Lewis acid sites (mmol•g^{-1})[h]	0.09	0.03	0.02	0.04	0.02	0.01
Brønsted/Lewis acidity	3.0	2.5	1.7	6.5	4.7	1.3

[a]determined using argon physisorption and NL-DFT method [28]; [b]obtained from N_2 physisorption and *t-plot* method; [c]obtained from N_2 physisorption and BJH analysis of adsorption branch; [d]obtained from N_2 physisorption; [e]determined from NH$_3$-TPD in desorption range 100–600 °C; [f]Determined with XRF; [e]determined with ^{29}Si MAS NMR peak simulations; [f]from Pyridine-IR, baseline-to-baseline integration of 1545 cm^{-1}; [g]from Pyridine-IR, baseline-to-baseline integration of 1455 cm^{-1};
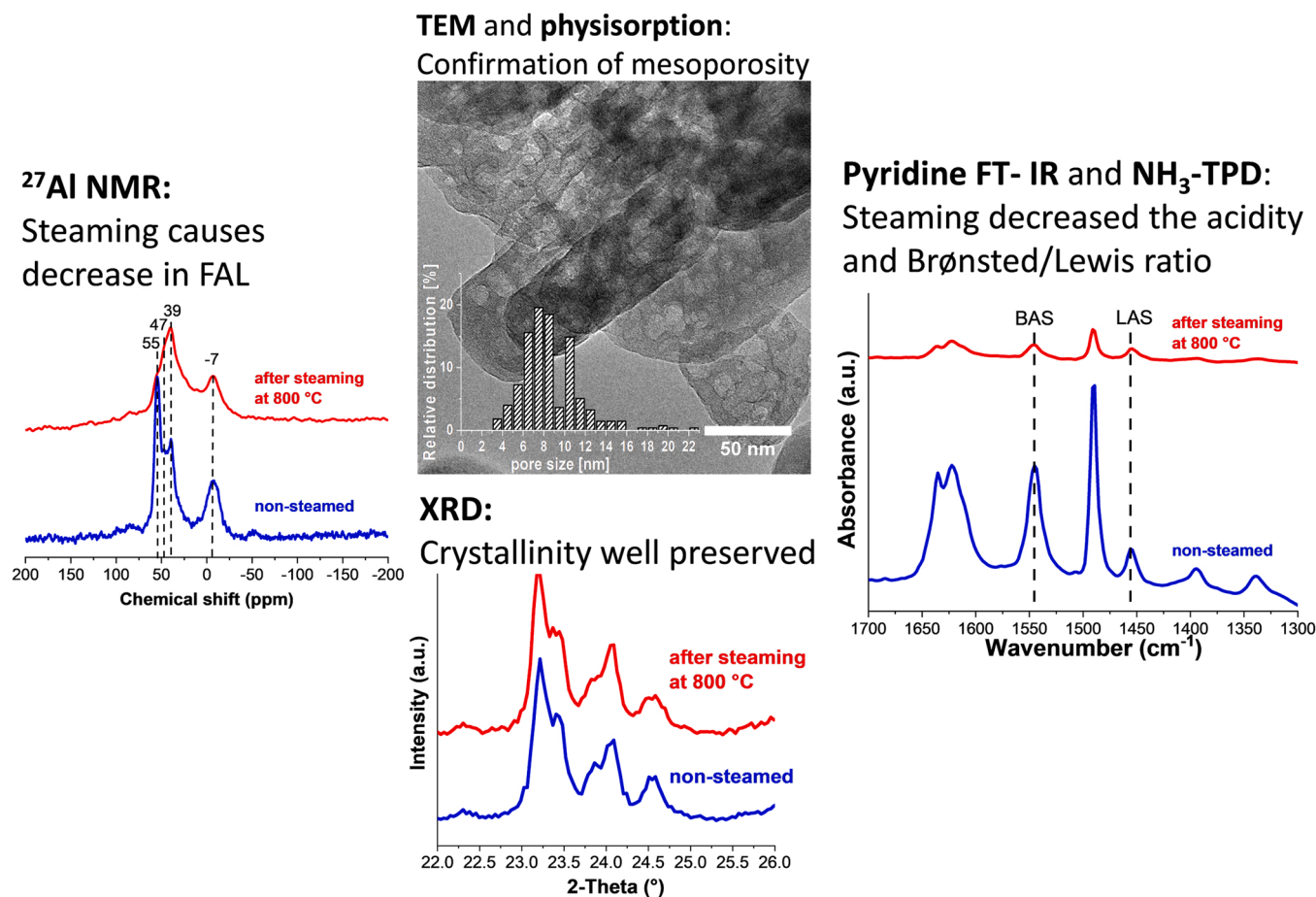
Fig. 1. Main catalyst characteristics summarized for *P/mesoZ55*.

450–650 °C while a severe decrease in acidity results [66–68]. After steaming at 800 °C, decreases in crystallinity to 90–95% of the crystallinity determined for the P-modified sample were reported by other researchers [53,69].

The phosphorus weight loading determined by XRF of the prepared samples ranged from 1.4 to 2.0 wt%. This range was reported favourable for maximum retention of strong acid sites after steam treatment [37,40,50] and improved propylene selectivities in alkene cracking [51–53].

Ammonia-TPD characterization (Fig. S5) revealed that mild steaming of *P/mesoZ30* produced a catalyst with 55% acidity of the unmodified parent *Z30*. After an additional more severe steam treatment at 800 °C, the acidity reduced to 0.15 mmol NH_3/g, corresponding to 18% of the acidity of *Z30*. The severely steam-treated *P/Z55-ss* and *P/mesoZ55-ss* had acidities of 0.10 and 0.09 mmol NH_3/g, corresponding to 16% and 14% of a parent *Z55*. It is noteworthy that lower phosphorus loadings (1% instead of 2% for *P/Z55* and 0.6 instead of 1.4% of *P/mesoZ55*) led to 13–17% lower acidities after severe steam treatment, confirming that the higher loading was more favorable for the retention of acidity under high hydrothermal severity [37,40,50].

Comparing the hydroxyl region in the IR plot (Fig. S6a+b) demonstrates clearly that the parent *Z55* and *Z30* contained a large amount of Brønsted acid sites (~3610 cm^{-1}), that was severely diminished after phosphorus modification and steaming. Furthermore, in the phosphorus containing samples a new band was observed that was earlier attributed to hydroxyl groups attached to phosphorus [37]. In line with the reduced acidity determined by NH_3-TPD, quantifying the Brønsted and Lewis acid sites after pyridine adsorption at 150 °C (Fig. 1, Fig. S7a+d) confirms that after P-modification and steam treatment, the total amount of Brønsted and Lewis acid sites had decreased considerably, particularly after the severe steam treatment at 800 °C. The loss in

Brønsted acidity after P-modification and steaming is more pronounced compared to the reduction in Lewis acidity, resulting in decreased ratios of Brønsted/Lewis acidity (Table 1).

As shown in Fig. S8, the as-prepared *P/mesoZ30* and *P/mesoZ55* showed AlO_4 framework aluminum atoms (FAL) as a sharp peak at ~55 ppm in the ^{27}Al NMR spectra [39,70,71]. While for HZSM-5 without P-modification, often a peak at 0 ppm is observed corresponding to AlO_5 and AlO_6 extra-framework aluminum atoms (EFAL) [52,71]. For the P-modified sample, a broader peak is observed at − 7 ppm for *P/mesoZ55* and at − 9 ppm for *P/mesoZ30*. This peak was also observed by other researchers for a HZSM-5 modified with 2 wt% P, and it appeared at − 12 ppm for a P loading of 4 wt% [39], indicating an effect of weight percentage on the peak position. A similar peak at − 9 ppm was observed by Zhao et al. [52] for HZSM-5 with 1.5 and 2 wt% P and these researchers attributed this resonance to AlO_6 coordinated to a phosphorus atom. The broad resonance between 40 and 10 ppm observed for the desilicated steam-treated samples (*P/mesoZ55-ss and P/mesoZ30-ss*) is usually assigned to extra-framework penta-coordinated AlO_5, but has also been assigned to a variety of local silico-aluminophosphate (SAPO) interfaces that formed when phosphoric acid binds with partially dislodged FAl species during the calcination after P modification [39,72]. The signals between 50 and 40 ppm are attributed to distorted framework or non-framework Al sites as a result of the desilication and P-modification [70]. After the steaming treatment at 800 °C, for both *P/mesoZ30-ss* and *P/mesoZ55-ss* there is a clear decrease in the peak intensity at 55 ppm assigned to well-ordered FAL species, with a corresponding increase in signal contribution between 20 and 30 ppm (Fig. 1). This agrees well with the observed increase in framework Si/Al as determined by ^{29}Si MAS NMR, and shows that the steam-treatment induces a dealumination of the zeolite

framework [70,73]. The broader resonance at ~40 ppm seem to be less affected by the steam treatment, in agreement with observations by others [39,72,74].

^{31}P NMR spectra (Fig. S9) show a broad response in a broad chemical shift range between 0 and −40 ppm due to the complicated environment of the phosphorus species in the samples [51]. After P modification but prior to steaming, *P/mesoZ30* showed a resonance at −6 ppm, attributed to the terminal phosphorus atoms in $H_4P_2O_7$ species not reacted with the framework aluminum [52,72,75,76]. The resonance at around −14 ppm may be attributed to the middle phosphorus atoms in

polyphosphates [77]. After steaming, the signals at −6 ppm, attributed to P in $H_4P_2O_7$ or terminal groups of polyphosphates non-attached to Al, disappeared, while the signals at −25, −30, and −39 ppm increased. These may be attributed to $AlPO_4$ or $(SiO)_xAl(OP)_{4−x}$ species, indicating that phosphorus interacted with aluminate species during the steam treatment [52]. A broad resonance centred around −24 ppm was also found by Van der Bij after steaming for a 2 wt% P/HZSM-5 and attributed to the formation of Al-O-P monodentate species [39].
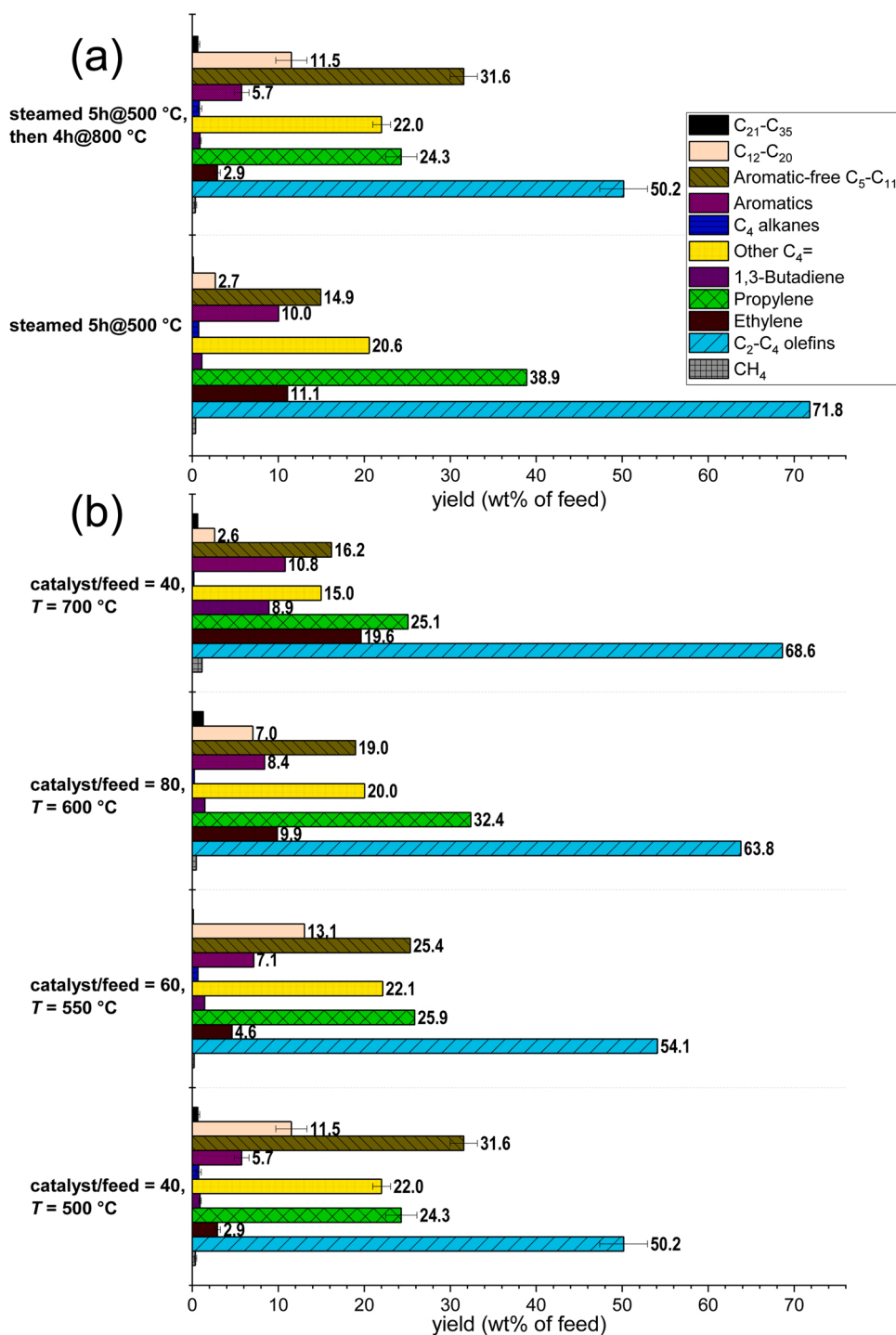

Fig. 2. Yield structure from upgrading LDPE pyrolysis vapors. (a) Comparing effect of steaming severity when using *P/mesoZ30-ms* and *P/mesoZ30-ss* at a catalyst temperature of 500 °C and a catalyst/feed ratio of 40. (b) Testing *P/mesoZ30-ss* at different temperatures and catalyst/feed ratios. Error bars are based on the standard deviation from four repetitions. Legend in (a) also applies for (b).

3.2. Catalyst screening for maximum C_2-C_4 olefin yield

3.2.1. Noncatalytic Reference

Product yields when the second reactor contained no catalyst but was either operated empty (at 375 °C) or filled with α-Al_2O_3 (at 600 °C) have been reported previously using LDPE and MPO as the feed [57]. An example two-dimensional GC chromatogram illustrating the products observed when conducting LDPE pyrolysis at 500 °C and passing the vapors over a bed of α-Al_2O_3 at 600 °C is shown in Fig. S10 and an exemplary yield structure for all individual compounds observed with MPO feed are found in Table S7. For pyrolysis of different virgin polyolefins, ~0.1 wt% CO was detected, indicating the presence of a small amounts of oxygen in the feed, and ~0.2 wt% oxygen in the feed was also reported by others for virgin PE [78,79]. Using MPO as feed and maintaining α-Al_2O_3 at 600 °C produced 1.1 wt% CO_2, 0.3 wt% CO and 0.04 wt% H_2. The higher presence of carbon oxides is attributed to the deoxygenation of PET contamination with a higher extent of decarboxylation over decarbonylation [60]. The higher yield of aromatics for MPO (Table S2) was attributed to the presence of polystyrene while the higher yield of C_5-C_{20} paraffins was attributed to the presence of PP, which is known to yield highly branched aliphatics in this range. The yield of the GC-quantifiable C_1-C_{35} fraction was ~70 wt% using LDPE as feed and ~80 wt% with MPO. The yield of C_{21+} waxes, calculated by difference in the mass closure, is in the same range with values reported by others(~50 wt% at 600 °C) [12]. The lower C_{21+} wax yield observed for MPO compared to LDPE is attributed to the higher yield of aromatics and, considering the increased yield of C_5-C_{20} aliphatics, possibly slightly enhanced cracking reactions facilitated by the inorganics present in the MPO feed.

3.2.2. In-line catalytic cracking with catalysts steamed at different severity

Passing LDPE pyrolysis vapors through a mildly steamed *P/mesoZ30-ms* catalyst at a reaction temperature of 500 °C completely converted the C_{21}-C_{35} light waxes and produced ~70 wt% C_2-C_4 olefins and 10 wt% aromatics (Fig. 2a). However, after an additional, higher severity steam treatment of the same catalyst at 800 °C, more C_{5+} aliphatics directly derived from the thermal pyrolysis in the first reactor remained in the product slate, and only ~50 wt% C_2-C_4 olefins and ~5 wt% aromatics were produced (Fig. 2a). The lower conversion is attributed to the lower acidity of the more severely steamed *P/mesoZ30-ss*,. (Table 1). While increased yields of aliphatics in the C_5-C_{20} range may be suitable for the co-production of transportation fuels, the goal of the present work was to maximize monomer recovery. By increasing catalyst temperature and/or catalyst loading, the cracking severity using the severely steamed *P/mesoZ30-ss* catalyst could be further increased (Fig. 2b), producing close to 70% C_2-C_4 olefins and 11 wt% aromatics at a catalyst/feed ratio of 40 and a reaction temperature of 700 °C. However, compared to using the mildly steamed *P/mesoZ30-ms* at an upgrading temperature of 500 °C (Fig. 2a), which produced a similar overall yield of C_2-C_4 olefins, the distribution of the light olefins was different with more ethylene and 1,3-butadiene and less propylene and other C_4 olefins produced when using *P/mesoZ30-ss* at 700 °C.

Even after phosphorus modification and steam treatment, *P/mesoZ30-ss* showed a high aromatization activity at all temperatures and

catalyst/feed ratios with high concentrations of two and three-ring aromatics present in the product slate (see Fig. S11). This is attributed to the fairly high Al content of the SiO_2/Al_2O_3 = 30 starting material resulting in a high density of acid sites. To proof this point, a mesoporous HZSM-5 with a lower acid site density that was derived from desilication of parent SiO_2/Al_2O_3 = 55 and subsequently modified with a similar P/Al ratio of ~0.6 and subjected to severe steaming at 800 °C was tested. And indeed, this *P/mesoZ55-ss* catalyst with lower acid site density showed a more favorable yield structure, producing virtually no higher C_{10+} aromatics (Figs. S12) while producing more propylene and C_4 olefins (Table 2). Therefore, in the following, the *P/mesoZ55-ss* was chosen as the best performing catalyst to study the effect of catalyst temperature and using different feeds on the production of monomers.

With increasing reaction temperature, the yield of CH_4, ethylene, 1,3-butadiene, and aromatics increased while there was a decreasing trend for C_{5+} aliphatics (Fig. 3). This was particularly pronounced between 600 and 700 °C, since the yield of benzene increased slightly from 0.9 wt% at 500 °C to 1.4 wt% at 600 °C but then more than doubled to 3.8 wt% at 700 °C. Similar trends are observed for ethylene and 1,3-butadiene (Fig. 3). Also the yield of H_2 first increased from 0.05 wt% (500 °C) to 0.11 wt% (600 °C), and then jumped to 0.30 wt% at 700 °C. H_2 yields often correlate with the yields of coke and aromatics (=coke precursors) due to their lower H/C ratio compared to the feed. Interestingly, propylene yield seemed less affected and likely even higher catalyst temperatures (or higher activity in terms of higher acid site density and/or strength) would have been needed to further crack propylene. The results presented in Fig. 2 and Fig. 3 illustrate that the catalyst/feed ratio and the catalyst temperature are important levers that affect the proportion of the different monomers. In the envisioned integrated catalytic fast pyrolysis process for direct production of valuable base chemicals, this provides flexibility for plant operators to favor the production of C_4 olefins, ethylene, propylene, or aromatics according to the highest market demand, all while keeping carbon losses to CH_4 and coke (see section *Catalyst stability and coking tendency*) reasonably low.

3.2.3. Impact of feedstock composition on product distribution

For the best catalyst P/mesoZ55-ss the product yields were evaluated for a whole range of potential feedstock compositions. As shown in Table 3, the product yield distribution using different PE-types was comparable, while there were also clear differences. In particular, from LLDPE ~10 wt% more propylene was produced compared to LDPE. On the other hand, upgrading of HDPE pyrolysis vapors produced the highest yield of C_4 olefins. Using PP as the feed resulted in a lower yield of C_4 olefins while C_5-C_{20} aliphatics were more prevalent. In contrast to PE, these aliphatics comprised more branched isomers as a consequence of the branched structure of PP and in agreement with findings from literature [80–85]. The yield structure obtained from the synthetic polyolefins mixture matched the expected composition of its constituents and ~85% monomers, i.e., ~80% C_2-C_4 olefins and ~5% aromatics were produced. With MPO as feed, the monomer production was slightly lower with 73 wt% C_2-C_4 olefins and ~9 wt% aromatics, primarily attributed to the higher aromatics content in the feed (from PET/PS contamination), which are more difficult to crack. It is worth noting that

Table 2
Product distribution using LDPE as feed and steamed phosphorous-modified mesoporous HZSM-5 obtained from parent materials with different SiO_2/Al_2O_3 ratios. Catalyst temperature = 600 °C and catalyst/feed ratio = 80. Yields obtained with α-Al_2O_3 instead of catalyst shown as non-catalytic reference.

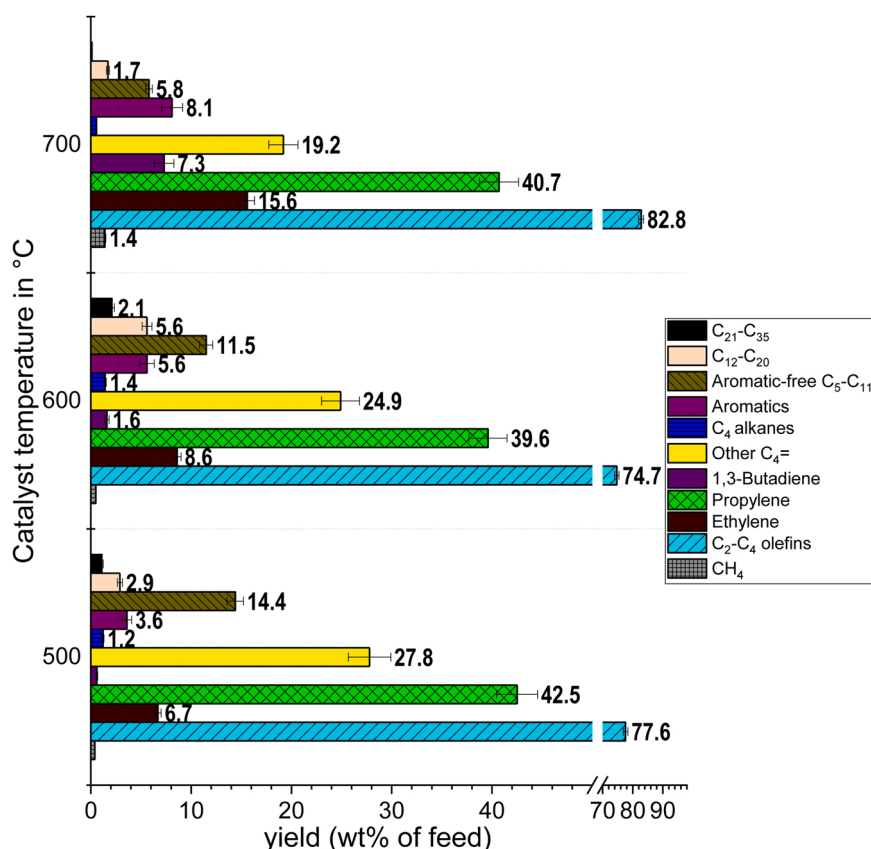| catalyst	CH_4	C_2-C_4 olefins	Ethylene	Propylene	1,3-Butadiene	Other C_4=	C_4 alkanes	Aromatics	Aromatic-free C_5-C_{11}	C_{12}-C_{20}	C_{21}-C_{35}
none (α-Al_2O_3)	0.5	8.2	3.0	2.7	0.5	1.7	0.8	1.9	14.3	20.5	53.7 *
P/mesoZ30-ss	0.5	63.6	9.9	32.3	1.5	20.0	0.3	8.4	18.9	7.0	1.3
P/mesoZ55-ss	0.4	73.7	8.5	39.1	1.6	24.5	1.4	5.5	11.3	5.5	2.1

[a]determined by difference in mass closure

Fig. 3. Yields obtained for a single run using LDPE as feed and *P/mesoZ55-ss* as catalyst at different catalyst temperatures. Catalyst loading was 32 mg and catalyst/feed ratio = 80.

Table 3
Yields obtained for a single reaction with different feeds using *P/mesoZ55-ss* as catalyst at 600 °C and a catalyst/feed ratio of 80.

feed	CH$_4$	C$_2$-C$_4$ olefins	Ethylene	Propylene	1,3-Butadiene	Other C$_4$=	C$_4$ alkanes	Aromatics	Aromatic-free C$_5$-C$_{11}$	C$_{12}$-C$_{20}$	C$_{21}$-C$_{35}$
LDPE	0.4	73.7	8.5	39.1	1.6	24.5	1.4	5.5	11.3	5.5	2.1
LLDPE	0.4	83.6	5.6	51.0	2.2	24.8	1.1	4.2	7.7	2.7	0.3
HDPE	0.3	82.8	7.1	37.2	2.6	36.0	0.9	4.1	9.9	1.6	0.4
PP	0.7	70.0	11.2	37.9	1.4	19.5	0.6	6.8	13.3	8.0	0.5
Synth. Mix[a]$_{measured}$	0.6	78.8	6.8	41.3	2.1	28.6	0.7	5.0	11.4	3.4	0.01
Theoretical mixture[b]	0.5	77.2	8.5	40.8	2.0	26.0	0.9	5.3	10.9	4.7	0.5
MPO[c]	0.7	73.2	12.1	38.5	1.6	21.0	1.0	9.0	10.3	4.5	1.3

[a] composition: 23 wt% LLDPE, 7.5 wt% LDPE, 29.5 wt% HDPE, 40 wt% PP;
[b] calculated based on the yields observed with bare polymers and their content in the prepared physical mixture
[c] post-consumer mixed polyolefins after waste sorting, cold-washing, and pelletization

the co-produced C$_5$-C$_{11}$ aliphatics (at ~10 wt%) and C$_{12+}$ products (at ~5 wt%) comprise primarily alkanes and therefore could be further converted to monomers via steam cracking or recycling to the catalyst reactor. Importantly, the pyrolysis-upgrading process provides higher P/E ratios compared to steam cracking, e.g., while the P/E ratios in steam cracking are ~0.65 and 0.53 for gas oil and naphtha, respectively [16], in the present work P/E ratios of 1.3–1.6 were obtained at a catalyst temperature of 700 °C and P/E ratios as high as ~8 resulted at a catalyst upgrading temperature of ~500 °C.

It has to be acknowledged that also a microporous *Z55* (without desilication treatment) that was impregnated with 2 wt% P and steam-treated at 800 °C (*P/Z55-ss*) showed a very similar yield distribution as what was obtained with *P/mesoZ55-ss* (Table S3). As such, there was no apparent benefit (in terms of improved monomer yields) of the added mesoporosity when comparing the product yield structure obtained with fresh, i.e., non-coked, microporous *P/Z55-ss* and hierarchical *P/mesoZ55-ss*. If the time-on-stream of the catalyst would be very short followed by catalyst regeneration—as is the case in fluid catalytic cracking—*P/Z55-ss* will be the preferred catalyst formulation as it does not require the additional treatment steps that are associated with introducing mesopores to the parent, microporous zeolite. However, for a longer time on stream—as would be the case in a fluid or fixed bed—the risk that large fractions of active sites inside the zeolite particle centers become inaccessible upon coke deposits blocking pore mouths may be higher in *P/Z55-ss* than in the hierarchical *P/mesoZ55-ss*.

3.2.4. Catalyst stability and coking tendency

In an attempt to study the deactivation of *P/Z55-ss*, repeated pyrolysis vapor pulses (derived from HDPE) were passed through the catalyst operated at 700 °C and a catalyst/feed ratio of 80, since a higher coking propensity was expected at the increased cracking severity based on the presence of aromatics as coke precursors (Fig. 3). However, no

deactivation of *P/Z55-ss* was observed after passing 16 pyrolysis vapor pulses over the catalyst, amounting to a cumulative feed/catalyst ratio of 0.2 (Table S4). The accumulated coke yield was 1.0 wt%, corresponding to a coke/catalyst loading of 0.2 wt%, or 5.1 µg coke/m^2 catalyst. Advantageously, even at the 16th run a high selectivity to a limited number of products was maintained, namely C$_2$-C$_4$ olefins, monoaromatics, and few C$_5$-C$_{20}$ aliphatics. These aliphatics were primarily alkanes, in stark contrast to thermal pyrolysis where the products contain a high concentration of α-olefins and di-olefins with unsaturation at both ends of the linear chain (α,ω-olefins). Despite the higher catalyst temperature of 700 °C, the formed aromatics mainly comprised monoaromatics (primarily benzene and toluene, and few alkylated monoaromatics (Fig. S12). No higher two and three-ring aromatics were observed, while these were already observed for *P/mesoZ30-ss* at a much lower cracking severity (Fig. S11), i.e. at 600 °C and catalyst/feed ratio = 40 vs. 700 °C and catalyst/feed ratio = 80. This reiterates the importance of using a catalyst with an acid site density lower than *P/mesoZ30-ss* and preparing the catalyst from a starting material with higher Si/Al, as was the case for *Z55* Table 1), appears crucial in limiting or even preventing the formation of higher aromatics.

Even at an 8 times lower catalyst loading (catalyst/feed ratio = 10) and when repeating 21 runs, i.e., reaching a cumulative feed/catalyst ratio of 2.1, no change in product distribution due to deactivation by coking was observed (Table S5). Under these conditions, due to the higher cumulative feed/catalyst ratio, more coke had accumulated on the catalyst, amounting to 0.6 wt% of the catalyst weight and 16 µg coke/m^2 catalyst. The coke yield, however, was only 0.3 wt% (vs. 1 wt% described above for catalyst/feed ratio = 80 and cumulative feed/

catalyst ratio = 0.2) due to the lower conversion at the lowered catalyst loading.

Comparing the product distribution obtained with catalyst/feed ratio = 80 (Table S4) and catalyst/feed ratio = 10 (Table S5) shows that at a lower catalyst/feed ratio (corresponding to a shorter contact time), the yield of C$_{12+}$ products was higher, while the higher catalyst/feed ratio allowed to crack these. This resulted in ~10 wt% higher ethylene yields, while also a small improvement (+ ~5 wt%) in propylene yield was observed (Table S4 and Table S5). The yield of C$_4$ olefins (excl. 1,3-butadiene), however, was lower at the higher catalyst/feed ratio, suggesting that these may have cracked to ethylene or reacted further, e.g., with ethylene and propylene forming aromatics during Diels-Alder reaction. The higher yield of aromatics observed at the higher catalyst/feed ratio agrees with the higher coke yield since aromatics are coke precursors. It is worth noting that a high catalyst temperature such as 700 °C may assist in thermally cracking the waxes and therefore effectively delay the catalyst deactivation. A change in product distribution due to catalyst deactivation by coke may therefore more easily be studied at a moderate catalyst temperature and using a feed with a high coking propensity. Therefore, in the next approach, MPO was used as a feed since its contamination with other plastics such as PET, PS, and PA was expected to form more coke on the catalyst than with virgin PE/PP [86,87]. Product yields as function of increasing run number were compared at a catalyst temperature of 600 °C using 8 mg unmodified parent *Z55* and 32 mg *P/Z55-ss* as catalyst. The difference in loading was required to obtain a similar level of conversion over the fresh catalyst, since *P/Z55-ss* had a lower acidity of 0.10 mmol NH$_3$/g compared to *Z55* (0.65 mmol NH$_3$/g). It is noted that the number of acid sites loaded to
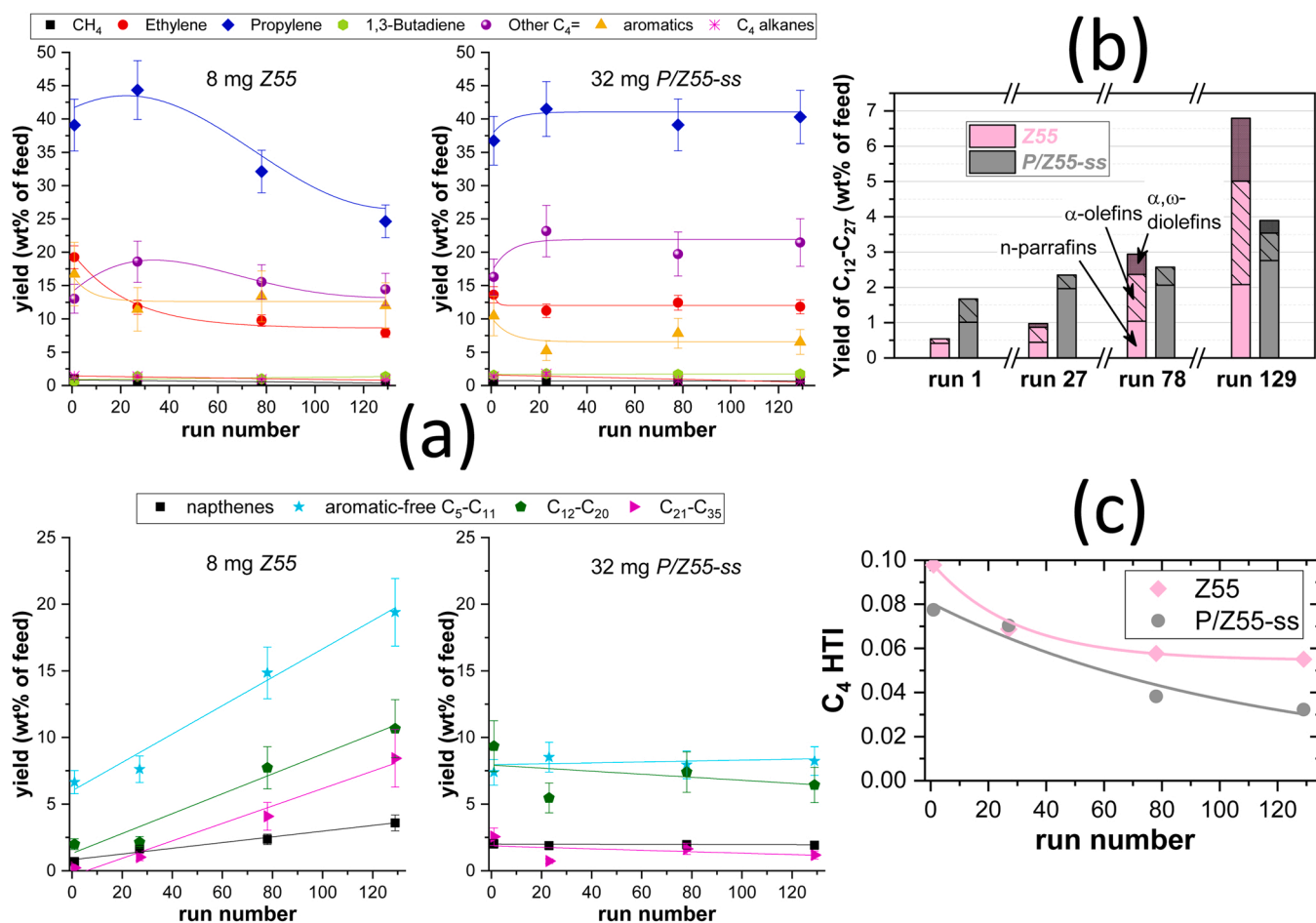

Fig. 4. (a) Product yields for increasing run numbers using either 8 mg of the parent unmodified *Z55* or 32 mg of *P/Z55-ss*. Yields are shown based on ash-free feed. The fitted lines are guides to the eye. (b) Yields of C$_{12}$-C$_{27}$ *n*-paraffins, α-olefins, and α,ω-diolefins. (c) C$_4$ hydrogen transfer index.

the reactor was still 58% higher using 8 mg *Z55* compared to using 32 mg *P/Z55-ss*. Despite this difference, the yields were remarkably constant during 130 runs when using *P/Z55-ss* while *Z55* rapidly lost its activity for converting C_{5+} aliphatics (Fig. 4). Likewise, there was a steeper decline in the yield of C_2-C_4 olefins, particularly propylene, compared to the stable yield profiles obtained with *P/Z55-ss*. For both catalysts, it is interesting to note an initial increase in propylene and C_4 olefins, while ethylene and aromatics are highest for the first run and then stabilize or decrease at a low rate with increasing run numbers. This may be attributed to higher coking rates and/or overcracking of the C_3/C_4 olefins over a fresh catalyst. The yields of CO_2, CO, and H_2 during the deactivation studies shown in Fig. 4 were ~2 wt%, 0.6 wt%, and 0.1 wt%, respectively, approximately double the values observed with α-Al$_2$O$_3$. Considering the low coke yields (vide infra), this shows that the maximum error made by normalizing the results without taking into account carbon oxides, H_2, and coke is ~3%.

Comparing the deactivation behavior of *P/mesoZ55-ss* with *P/Z55-ss* (Fig. S13) shows that initially there was a slight decline in C_2-C_4 olefins using *P/mesoZ55-ss,* and after that, both catalysts displayed rather stable operation. This indicates that only the initialization behavior of these catalyst is different. To draw conclusions on stability, future studies should monitor the product yields over time for continuous and longer operation until there is a steep decline in activity observed.

The catalytic upgrading significantly decreased the yield of higher α-olefins and α,ω-diolefins (unsaturation in the alpha and end position) compared to the thermal reference case (Fig. S10). This can be explained by the higher reactivity of α-olefins and dienes since the end-chain unsaturation provides high electron density and little steric limitations, thereby facilitating reaction with acid sites. While for *Z55* the selectivity to *n*-paraffins rapidly declined with increased run number at the expense of α-olefins and dienes, the selectivity to *n*-paraffins remained high and only at run number 130 some dienes were observed in the product slate (Fig. 4b). Alkanes may potentially also result from hydrogen transfer reactions, and there was a decreasing trend in the C_4 hydrogen transfer index (HTI) (Fig. 4c)—defined as the combined yields of iso-butane and *n*-butane divided by the total yield of C_4 alkanes and alkenes [88,89]. Generally, however, the extent of hydrogen transfer is quite low in the *ex-situ* vapor phase upgrading since hydrogen transfer as an exothermic reaction with a slow reaction rate is not favoured by the high reaction temperature and short reaction time [90]. For in-situ catalytic upgrading with the polymer melt in direct contact with the catalyst, higher HTI values of ~0.2–0.4 were reported when using HZSM-5 in fluid bed reactors [91,92].

Even though a lower amount (8 mg) of *Z55* was loaded to obtain a similar initial conversion of C_{12+} products as with 32 mg of *P/Z55-ss*, after 130 runs the coke yields using 8 mg *Z55* was very similar with 0.17 wt% compared to 0.20 wt% using 32 mg *P/Z55-ss*. This clearly demonstrates the higher coking propensity of the unmodified parent *Z55*, particularly apparent when comparing the coke deposited per surface area, which was 8 μg/m^2 using P/Z55-ss and 27 μg/m^2 for the parent *Z55*. This can explain the faster loss in activity observed for the parent *Z55* (Fig. 4). Finally, it is worth noting that for catalysts that were steam-treated under high severity (800 °C), there was no loss in activity apparent for repeated cycles of reaction (at 600 °C) and oxidative regeneration (at 700 °C), as shown in Table S6.

3.3. Plantwide process evaluation

The performance of the studied catalytic pyrolysis of plastic waste streams to valuable base chemicals was further evaluated in a plantwide context. Particularly, the energy and carbon footprint of the direct catalytic process studied in the present work at a catalyst temperature of 600 °C (=Case 1) were estimated and compared against the conventional two-step counterpart (Case 2) comprising pyrolysis of the plastic waste streams followed by pyrolytic oil steam cracking. To this end, detailed process flow diagrams (PFDs) of the reaction section were developed for both cases and optimized with respect to heat minimization. Beside fossil-based heating (provided by fired heaters), electrically conductive heating (applied by electrified heaters) was also considered in the analysis. The latter constitutes a modern and efficient alternative that can (potentially) fully run on renewable electricity, thereby, preventing direct CO_2 emissions sourced by fuel combustion [93]. The respective PFDs after application of heat integration are presented in the supplementary material (Fig. S14-Fig. S17).

The following analysis was performed on the basis of i) the feed: 1 kg of plastic waste; polyethylene was considered as a model compound and ii) the final product: 1 kg of high value chemicals (HVC) comprising a mixture of ethylene (C_2H_4), propylene (C_3H_6), benzene (C_6H_6), hydrogen (H_2) and butadiene (C_4H_6) to facilitate a fair benchmarking over other peer processes.

3.3.1. Energy footprint

A heat integration targeted to the reactors' energy duty minimization (i.e. catalytic reactor, pyrolyzer and steam cracker) was initially performed. A detailed description of the heat integration approach is given in the supplementary material. The energy footprints by means of total energy demand of the studied (Case 1) and conventional (Case 2) processes are presented in Fig. 5. Both fossil-based (Fig. 5a) and electrically conductive heating (Fig. 5b) alternatives are included while the contribution of each process step to the total energy demand is also presented in the supplementary material (Figs. S18 and S19). The former heating alternative always resulted in a higher total energy demand than the latter in both process cases. The reasoning lies in the higher heat losses occurring in the heating elements which subsequently drive the heater efficiency: 65.6% [94] and 95% [95] are representative efficiency values for the fired and electrified heaters, respectively. Although multiple heat exchangers are placed in series to further minimize the heat losses in the flue gas when fired heaters are used (Fig. S14 and S16), the high operating temperatures (usually higher than that of the flue gas) do not always allow for high heat integration potential. Notably, no flue gas is present when electrified heaters are used.

Collectively, 3.9 kJ$_{heat}$/kg$_{plastics}$ (7.4 kJ$_{heat}$/kg$_{HVC}$) and 6.4 kJ$_{heat}$/kg$_{plastics}$ (11.9 kJ$_{heat}$/kg$_{HVC}$) are required for Case 1 and Case 2, respectively, when fossil-based heating is applied, whereas 3.0 kJ$_{el.}$/kg$_{plastics}$ (5.7 kJ$_{el.}$/kg$_{HVC}$) and 4.3 kJ$_{el.}$/kg$_{plastics}$ (8.0 kJ$_{el.}$/kg$_{HVC}$) are required for Case 1 and Case 2, respectively, when electrically conductive heating is applied. Overall, in the studied process (Case 1), the energy duty is about 38% lower than in the conventional counterpart (Case 2) when fired heaters are employed and about 30% lower when electrified heaters are employed, showing that plastics cracking and catalytic upgrading integrated in one unit can lead to significantly reduced energy inputs.

3.3.2. Carbon footprint

Herein, a preliminary ex-ante life cycle assessment focusing on the process carbon footprint (expressed in kg CO_2-eq./kg) was performed on the basis of the energy demand that was reported in the previous section. The foreground data (i.e. energy demand) was linked to background data from the ecoinvent v3.6 database [96]. Background processes (i.e. electricity and heat supply) were mostly representative of European market (heat and electricity supply). The cut-off system model was applied [97]: the waste stream impacts were fully ascribed to the waste producer but the treatment activity impacts were attributed to the party that is in charge of the waste stream valorization since there is an economic interest (chemicals production). Following this reasoning, the plastic waste stream was considered burden-free while the energy demand associated to the treatment activity was charged on the foreground processes (Case 1 and Case 2). The catalyst synthesis carbon footprint was neglected [98].

The carbon footprint of both the studied (Case 1) and conventional (Case 2) processes considering fired heaters running on natural gas and electrified heaters running on grid, solar and wind harvested electricity
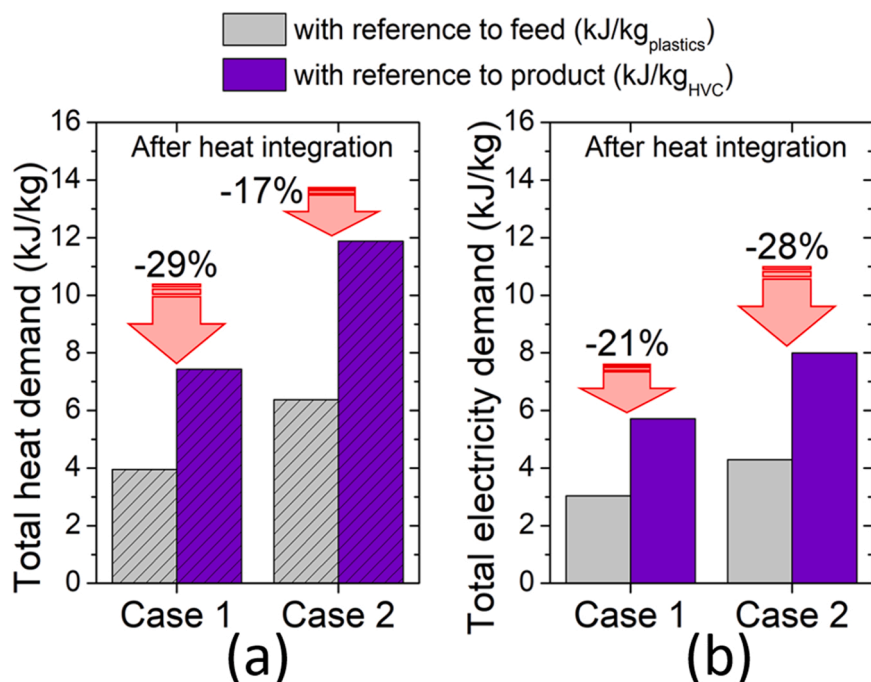
Fig. 5. Energy footprint by means of total energy demand of the studied (Case 1) and conventional (Case 2) processes after heat integration: a) use of fired heaters running on natural gas and b) use of electrified heaters. The downwards pointing arrows indicate the reducing in heat/electricity demand after heat integration, in comparison to the demand before heat integration.
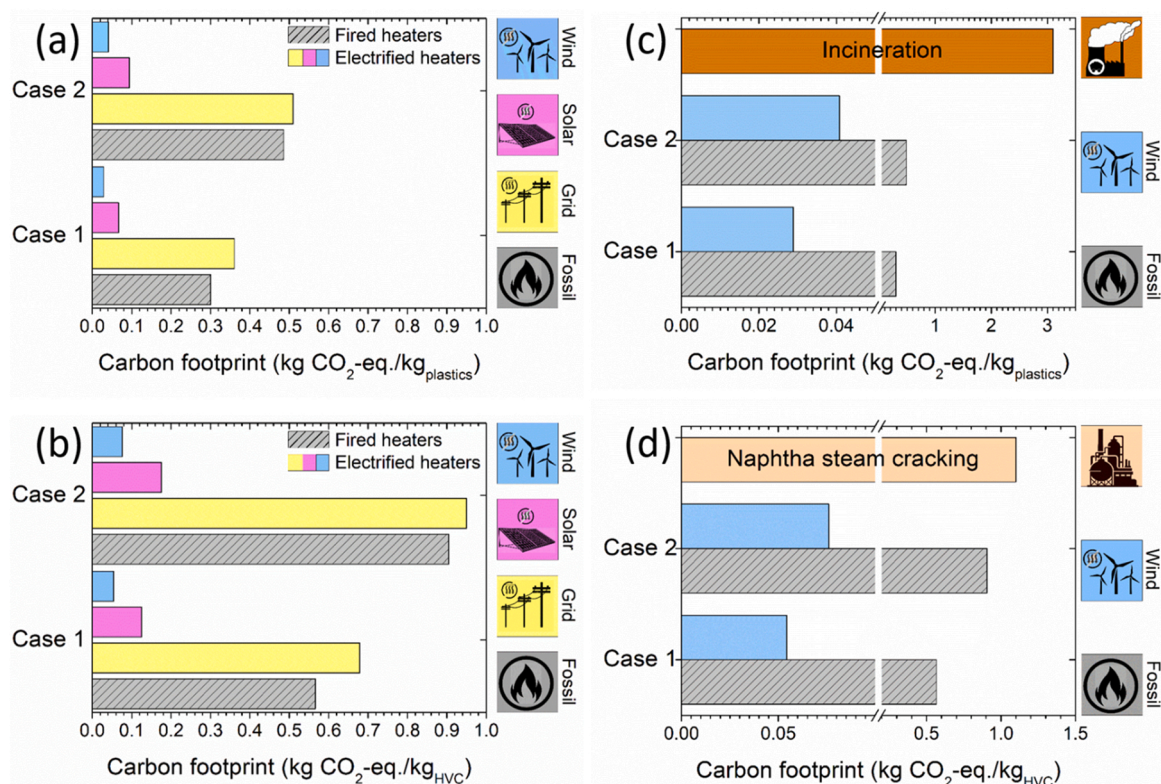

Fig. 6. Left: Carbon footprint of the studied catalytic fast pyrolysis (=Case 1) and steam cracking of plastic-waste derived pyrolysis oil (=Case 2) processes after heat integration for fired heaters running on natural gas and electrified heaters running on grid, solar and wind electricity: a) with reference to feed (expressed in kg CO_2-eq./kg$_{plastics}$) and b) with reference to product (expressed in kg CO_2-eq./kg$_{HVC}$). Right: Carbon footprint benchmarking of Case 1 and Case 2 processes for fired heaters and electrified heaters (running on wind electricity) against traditional peer processes: a) plastic waste streams incineration and b) high value chemicals synthesis via naphtha steam cracking.

is shown in Fig. 6 (Fig. 6a: with reference to feed; Fig. 6b:with reference to product). Both processes attain the highest carbon footprint (even higher than that of fossil-based heat as energy source) when grid electricity is utilized as energy source; specifically, 0.36 kg CO_2-eq./kg$_{plastics}$ (0.68 kg CO_2-eq./kg$_{HVC}$) and 0.51 kg CO_2-eq./kg$_{plastics}$ (0.95 kg CO_2-eq./kg$_{HVC}$) for Case 1 and Case 2, respectively. Although a mix of fossil fuels and renewable sources is considered in grid electricity generation, the unitary impact of grid electricity gets higher than that of fossil-based heat after applying the conversion efficiency (0.42 kg CO_2-eq./kWh$_{grid\ el.}$ versus 0.27 kg CO_2-eq./kWh$_{heat}$). Yet, both processes attain significantly low carbon footprint when renewable electricity solely drives the heaters: about 80% lower environmental burden is attained when solar harvested electricity is utilized instead of grid electricity. In case of wind harvested electricity utilization, the lowest carbon footprint is attained: 0.03 kg CO_2-eq./kg$_{plastics}$ (0.05 kg CO_2-eq./kg$_{HVC}$) and 0.04 kg CO_2-eq./kg$_{plastics}$ (0.07 kg CO_2-eq./kg$_{HVC}$) for Case 1 and Case 2, respectively. The unitary impact of solar harvested electricity is about two times the wind harvested one since higher environmental burden is imposed along the life cycle of a photovoltaic panel as compared to that of a wind turbine.

Next, a process benchmarking from an environmental perspective was conducted. The traditional plastic waste incineration (Fig. 6c) and naphtha steam cracking (Fig. 6d) were considered as benchmarks. Fig. 6c shows the environmental impacts of Case 1 and Case 2, as potential plastic waste valorization processes, in comparison to that of incineration. The functional unit for this comparison was 1 kg of plastic waste valorization, while a gate-to-gate approach was applied. Fig. 6d shows the environmental impacts of Case 1 and Case 2, as alternative processes for HVC synthesis, in comparison to naphtha steam cracking. The functional unit for this comparison was 1 kg of HVC synthesis, while a cradle-to-gate approach was applied. The carbon footprint value of the incineration process was calculated based on the plastic waste combustion reaction, assuming polyethylene as the main plastic waste stream (Table S8) and the carbon footprint value of the naphtha steam cracking was obtained from literature data [99] after considering an intermediate value (1.1 kg CO_2-eq./kg$_{HVC}$) between world-average and state-of-the-art processes.

Both Case 1 and Case 2 constitute far more sustainable (plastic waste) valorization process alternatives than the traditional incineration, regardless the primary energy source utilized (Fig. 6c). At least an order of magnitude lower carbon footprint can be attained when fired heaters running on natural gas are employed whereas, notably, two orders of magnitude lower carbon footprint can be attained if the fired heaters are replaced to electrified heaters running on wind harvested electricity. In all scenarios, the studied catalytic process (Case 1) results in the lowest possible environmental burden (Fig. 6c).

Fig. 6d shows the same trend when Case 1 and Case 2 are proposed for HVC synthesis. At least 45% and 15% reduction in the carbon footprint of Case 1 and Case 2, respectively, is attained when HVC are produced by plastic waste in fired heaters than oil-based naphtha in thermally driven steam crackers. Although a higher amount of energy is required to melt and crack the long carbon chains of the plastic waste as compared to naphtha steam cracking, a lower environmental impact is attained eventually. This is ascribed to the fact that plastic waste that serves as carbon source is burden-free, unlike oil-based naphtha which accounts for almost 30% of the total carbon footprint [99]. Remarkably, the environmental burden drops to an order of magnitude lower values upon switching to electrified heaters. Again, the proposed catalytic process (Case 1) results in the lowest possible environmental burden.

We note that an alternative to the proposed in-line catalytic cracking of pyrolysis vapors would be the thermal cracking, either directly in the pyrolysis reactor at higher temperatures, or operating the pyrolysis reactor at moderate temperatures (~500 °C) followed by thermally cracking the generated waxes in a downstream thermal cracking reactor. However, this approach requires high temperatures of ~750 °C to obtain light olefin yields of ~70% and is therefore characterized by increased energy demand and increased yields of CH_4 and ethylene at the expense of propylene [100–106]. Using a catalyst in the present work for vapor-phase upgrading allows obtaining at least 10 wt% higher propylene yields than what has been reported under thermal conditions.

Future work should study the heat integration of the proposed process to determine if the combustion of CH_4 and coke will provide sufficient process heat in continuous operation. Coke yields from upgrading polyolefins pyrolysis vapors are considerably lower than FCC cracking of heavy feed, where the combustion of the ~5–10 wt% of coke produced [107] provides enough heat to run the process (but also entails high unavoidable CO_2 emission). This was already recognized for steam catalytic cracking of naphtha at ~700 °C, for which the coke deposition was deemed too low to produce by combustion the catalyst temperatures required in the reactor [54]. Lastly, it is worth noting that it might be possible lowering the total costs and environmental footprint even further by producing the ZSM-5 zeolite from mining waste streams [108].

4. Conclusion

Unprecedently high olefin yields were obtained with a phosphorous-modified conventional and mesoporous HZSM-5 zeolite. They were demonstrated to be suitable catalysts for producing valuable base chemicals from different virgin and post-consumer waste polyolefins. After steam treatment at 800 °C, the acidity of the catalysts was reduced to ~0.10–0.15 mmol NH_3/g, resulting in a lower activity. However, these catalysts can be considered stable under reaction and regeneration conditions which are not expected to exceed 700 °C in the process of cracking plastics pyrolysis vapors. Varying the catalyst/feed ratio between 10 and 80 and the catalyst temperature between 500 and 700 °C affected the proportion of different monomer products. This provides great flexibility for plant operators to steer the product slate towards the highest market demand and maximize C_4 olefins, ethylene, propylene, or aromatics production, all while keeping carbon losses to CH_4 and coke below 1.5% and 1%, respectively.

The yield structure obtained from a synthetic polyolefins mixture of LLDPE, LDPE, HDPE and PP matched the relative contributions of the single polymers, and an extremely high monomer yield of 84 wt%, i.e., 79 wt% C_2-C_4 olefins and 5 wt% aromatics was obtained. When using post-consumer MPO feed, the monomer yield was slightly lower with 74 wt% C_2-C_4 olefins and 9 wt% aromatics, and this is attributed to the higher aromatics content in the feed from PS and the presence of some PET.

While parent HZSM-5 rapidly deactivated and showed a high coking propensity (27 µg of coke /m^2 catalyst), HZSM-5 that was modified with 2 wt% P and steam treated at 800 °C showed almost no deactivation during 130 runs with stable conversion of C_{5+} aliphatics and high C_2-C_4 olefins selectivity with a much lower coke deposition of 8 µg/m^2.

Finally, the studied catalytic process constitutes a sustainable alternative process for plastic waste valorization since it leads to about an order of magnitude (0.3 versus 3.1 kg CO_2-eq./kg$_{plastics}$) lower environmental burden than the current practice of incineration. In addition, it constitutes an excellent paradigm of circular economy by closing the carbon balance upcycle: plastic wastes are transformed to fresh building blocks (i.e. HVC) which can further be used for new polymers production, while this cycle can (theoretically) be repeated numerous times, hence avoiding downcycling issues observed in mechanical recycling. Future investigations should be directed to study the techno-economics and scale-up of the presented single-step process to benchmark it against steam cracking of pyrolysis-derived liquids.

Associated content

Supporting Information

Reactor scheme; Uncertainty assessment; NH3-TPD description and

desorption profiles; N$_2$ physisorption data; XRD characterization; FT-IR spectra of the OH-stretch region and after pyridine adsorption; ^{27}Al NMR spectra; ^{31}P NMR spectra; example GC×GC chromatograms for upgrading reactor filled with inert α-Al$_2$O$_3$ or different catalysts; catalyst stability of P/Z55-ss vs. P/mesoZ55-ss; methodology of heat integration approach and heat duty calculation; Process flow diagrams of Case 1 and Case 2 with heat supplied by fired heaters via combustion or electric resistances; Energy footprint of processes before heat integration; heat duty distribution; electricity duty contribution; Calculation of CO$_2$ emissions released by 1 kg of plastics combustion;.

CRediT authorship contribution statement

Dr. Andreas Eschenbacher: Investigation; Project administration; Writing – original draft; Visualization. **Dr. Robin John Varghese:** Investigation; Validation; Resources. **Dr. Evangelos Delikonstantis**: Investigation; Methodology; Writing – review & editing. Writing – original draft; Visualization. **Oleksii Mynko:** Investigation; Methodology; Writing – review & editing. **Dr. Farnoosh Goodarzi:** Investigation; Writing – review & editing. **Dr. Kasper Enemark-Rasmussen:** Investigation; Writing – review & editing. **Dr. Jogchum Oenema:** Investigation; Writing – review & editing. **Dr. Mehrdad Seifali Abbas-Abadi**: Writing – review & editing. **Prof. Georgios D. Stefanidis**: Resources; Supervision; Writing – review & editing. **Prof. Kevin M. Van Geem:** Funding acquisition; Resources; Supervision; Writing – review & editing; Methodology; Project administration.

Declaration of Competing Interest

The authors declare that they have no known competing financial interests or personal relationships that could have appeared to influence the work reported in this paper.

Acknowledgment

Author contributions

The manuscript was written through the contributions of all authors. All authors have given approval to the final version of the manuscript.

Appendix A. Supporting information

Supplementary data associated with this article can be found in the online version at doi:10.1016/j.apcatb.2022.121251.

References

[1] M. Worsdorfer, The future of petrochemicals, Futur. Petrochem. IEA (2018), https://doi.org/10.1787/9789264307414-en.

[2] D. Dickson, A. Hussain, B. Kumpf, The Future of Petrochemicals: Growth Surrounded by Uncertainty, 2019. ⟨https://fdocuments.in/document/the-future-of-petrochemicals-deloitte-united-states-2020–03-17-petrochemicals.html⟩ (accessed December 15, 2021).

[3] O. Awayssa, N. Al-Yassir, A. Aitani, S. Al-Khattaf, Modified HZSM-5 as FCC additive for enhancing light olefins yield from catalytic cracking of VGO, Appl. Catal. A Gen. 477 (2014) 172–183, https://doi.org/10.1016/j.apcata.2014.03.021.

[4] A. Akah, M. Al-Ghrami, Maximizing propylene production via FCC technology, Appl. Petrochem. Res. 5 (2015) 377–392, https://doi.org/10.1007/s13203-015-0104-3.

[5] X. Meng, C. Xu, J. Gao, L. Li, Studies on catalytic pyrolysis of heavy oils: reaction behaviors and mechanistic pathways, Appl. Catal. A Gen. 294 (2005) 168–176, https://doi.org/10.1016/j.apcata.2005.07.033.

[6] A.I. Hussain, A.M. Aitani, M. Kubů, J.ʁ Čejka, S. Al-Khattaf, Catalytic cracking of Arabian Light VGO over novel zeolites as FCC catalyst additives for maximizing propylene yield, Fuel 167 (2016) 226–239, https://doi.org/10.1016/j.fuel.2015.11.065.

[7] M. Roosen, N. Mys, M. Kusenberg, P. Billen, A. Dumoulin, J. Dewulf, K.M. Van Geem, K. Ragaert, S. De Meester, Detailed analysis of the composition of selected plastic packaging waste products and its implications for mechanical and thermochemical recycling, Environ. Sci. Technol. 54 (2020) 13282–13293, https://doi.org/10.1021/acs.est.0c03371.

[8] K. Ragaert, L. Delva, K. Van Geem, Mechanical and chemical recycling of solid plastic waste, Waste Manag 69 (2017) 24–58, https://doi.org/10.1016/j.wasman.2017.07.044.

[9] J.-P. Lange, Towards circular carbo-chemicals – the metamorphosis of petrochemicals, Energy Environ. Sci. (2021), https://doi.org/10.1039/d1ee00532d.

[10] K. Kleinhans, M. Hallemans, S. Huysveld, G. Thomassen, K. Ragaert, K.M. Van Geem, M. Roosen, N. Mys, J. Dewulf, S. De Meester, Development and application of a predictive modelling approach for household packaging waste flows in sorting facilities, Waste Manag. 120 (2021) 290–302, https://doi.org/10.1016/j.wasman.2020.11.056.

[11] J.-P. Lange, Towards circular carbo-chemicals – the metamorphosis of petrochemicals, Energy Environ. Sci. (2021), https://doi.org/10.1039/D1EE00532D.

[12] M. Arabiourrutia, G. Elordi, G. Lopez, E. Borsella, J. Bilbao, M. Olazar, Characterization of the waxes obtained by the pyrolysis of polyolefin plastics in a conical spouted bed reactor, J. Anal. Appl. Pyrolysis 94 (2012) 230–237, https://doi.org/10.1016/j.jaap.2011.12.012.

[13] W. Kaminsky, Chemical recycling of plastics by fluidized bed pyrolysis, Fuel Commun. 8 (2021), 100023, https://doi.org/10.1016/J.JFUECO.2021.100023.

[14] M. Kusenberg, A. Zayoud, M. Roosen, H.D. Thi, M.S. Abbas-Abadi, U. Eschenbacher, Andreas Kresovic, S. De Meester, K.M. Van Geem, A comprehensive experimental investigation of plastic waste pyrolysis oil quality and its dependence on the plastic waste composition, Fuel Process. Technol. 227 (2021), 107090, https://doi.org/10.1016/j.fuproc.2021.107090.

[15] M. Kusenberg, K.M.Van Geem, Opportunities and challenges for the application of post-consumer plastic waste pyrolysis oils as steam cracker feedstocks: to decontaminate or not to decontaminate, Waste Manag 138 (2021) 83–115.

[16] C. Dean, Naphtha catalytic cracking for propylene production, Digit. Refin. 18 (2013) 1–5. ⟨https://www.digitalrefining.com/article/1000787⟩.

[17] Recycling and the future of the plastics industry | McKinsey, (n.d.). ⟨https://www.mckinsey.com/industries/chemicals/our-insights/how-plastics-waste-recycling-could-transform-the-chemical-industry⟩ (accessed June 22, 2021).

[18] M. Solis, S. Silveira, Technologies for chemical recycling of household plastics – a technical review and TRL assessment, Waste Manag. 105 (2020) 128–138, https://doi.org/10.1016/j.wasman.2020.01.038.

[19] R. Palos, A. Gutiérrez, F.J. Vela, M. Olazar, J.M. Arandes, J. Bilbao, Waste refinery: the valorization of waste plastics and end-of-life tires in refinery units. a review, Energy Fuels. 35 (2021) 3529–3557, https://doi.org/10.1021/acs.energyfuels.0c03918.

[20] L.O. Mark, M.C. Cendejas, I. Hermans, The use of heterogeneous catalysis in the chemical valorization of plastic waste, ChemSusChem 13 (2020) 5808–5836, https://doi.org/10.1002/cssc.202001905.

[21] S.D. Anuar Sharuddin, F. Abnisa, W.M.A. Wan Daud, M.K. Aroua, A review on pyrolysis of plastic wastes, Energy Convers. Manag. 115 (2016) 308–326, https://doi.org/10.1016/j.enconman.2016.02.037.

[22] D.P. Serrano, J. Aguado, J.M. Escola, Developing advanced catalysts for the conversion of polyolefinic waste plastics into fuels and chemicals, ACS Catal. 2 (2012) 1924–1941, https://doi.org/10.1021/cs3003403.

[23] A. Eschenbacher, P.A. Jensen, U.B. Henriksen, J. Ahrenfeldt, C. Li, J.Ø. Duus, U. V. Mentzel, A.D. Jensen, Impact of ZSM-5 deactivation on bio-oil quality during upgrading of straw derived pyrolysis vapors, Energy Fuels 33 (2019) 397–412, https://doi.org/10.1021/acs.energyfuels.8b03691.

[24] A. Eschenbacher, P.A. Jensen, U.B. Henriksen, J. Ahrenfeldt, C. Li, J.Ø. Duus, U. V. Mentzel, A.D. Jensen, Deoxygenation of wheat straw fast pyrolysis vapors using HZSM-5, Al2O3, HZSM-5/Al2O3 extrudates, and desilicated HZSM-5/Al2O3 extrudates, Energy Fuels 33 (2019) 6405–6420, https://doi.org/10.1021/acs.energyfuels.9b00906.

[25] K.G. Kalogiannis, S.D. Stefanidis, A.A. Lappas, Catalyst deactivation, ash accumulation and bio-oil deoxygenation during ex situ catalytic fast pyrolysis of biomass in a cascade thermal-catalytic reactor system, Fuel Process. Technol. 186 (2019) 99–109, https://doi.org/10.1016/j.fuproc.2018.12.008.

[26] J.C. Groen, L.A.A. Peffer, J.A. Moulijn, J. Pérez-Ramírez, Mesoporosity development in ZSM-5 zeolite upon optimized desilication conditions in alkaline

medium, Colloids Surf. A Physicochem. Eng. Asp. 241 (2004) 53–58, https://doi.org/10.1016/j.colsurfa.2004.04.012.

[27] J.C. Groen, J. a Moulijn, J. Peréz-Ramírez, Desilication: on the controlled generation of mesoporosity in MFI zeolites, J. Mater. Chem. 16 (2006) 2121, https://doi.org/10.1039/b517510k.

[28] A. Eschenbacher, P.A. Jensen, U.B. Henriksen, J. Ahrenfeldt, S. Ndoni, C. Li, J. Ø. Duus, U.V. Mentzel, A.D. Jensen, Catalytic deoxygenation of vapors obtained from ablative fast pyrolysis of wheat straw using mesoporous HZSM-5, Fuel Process. Technol. 194 (2019), 106119, https://doi.org/10.1016/J.FUPROC.2019.106119.

[29] M. Holm, E. Taarning, K. Egeblad, C.H. Christensen, Catalysis with hierarchical zeolites, Catal. Today 168 (2011) 3–16, https://doi.org/10.1016/j.cattod.2011.01.007.

[30] D.P. Serrano, R.A. García, G. Vicente, M. Linares, D. Procházková, J. Čejka, Acidic and catalytic properties of hierarchical zeolites and hybrid ordered mesoporous materials assembled from MFI protozeolitic units, J. Catal. 279 (2011) 366–380, https://doi.org/10.1016/j.jcat.2011.02.007.

[31] D. Verboekend, M. Milina, S. Mitchell, J. Pérez-Ramírez, Hierarchical zeolites by desilication: occurrence and catalytic impact of recrystallization and restructuring, Cryst. Growth Des. 13 (2013) 5025–5035, https://doi.org/10.1021/cg4010483.

[32] J. Garcia-Martinez, K. Li, Mesoporous zeolites: preparation. Characterization and Applications, Wiley-VCH Verlag GmbH & Co KGaA,, 2015.

[33] M.A. Bari Siddiqui, A.M. Aitani, M.R. Saeed, S. Al-Khattaf, Enhancing the production of light olefins by catalytic cracking of FCC naphtha over mesoporous ZSM-5 catalyst, Top. Catal. 53 (2010) 1387–1393, https://doi.org/10.1007/s11244-010-9598-1.

[34] A. Eschenbacher, F. Goodarzi, A. Saraeian, S. Kegnæs, B.H.B.H. Shanks, A.D.A. D. Jensen, Performance of mesoporous HZSM-5 and Silicalite-1 coated mesoporous HZSM-5 catalysts for deoxygenation of straw fast pyrolysis vapors, J. Anal. Appl. Pyrolysis 145 (2019), 104712, https://doi.org/10.1016/J.JAAP.2019.104712.

[35] A. Eschenbacher, J.A. Andersen, A.D. Jensen, Catalytic conversion of acetol over HZSM-5 catalysts – influence of Si/Al ratio and introduction of mesoporosity, Catal. Today (2020), https://doi.org/10.1016/j.cattod.2020.03.041.

[36] L.Y. Jia, M. Raad, S. Hamieh, J. Toufaily, T. Hamieh, M.M. Bettahar, G. Mauviel, M. Tarrighi, L. Pinard, A. Dufour, Catalytic fast pyrolysis of biomass: Superior selectivity of hierarchical zeolites to aromatics, Green. Chem. 19 (2017) 5442–5459, https://doi.org/10.1039/c7gc02309j.

[37] T. Blasco, A. Corma, J. Martínez-Triguero, Hydrothermal stabilization of ZSM-5 catalytic-cracking additives by phosphorus addition, J. Catal. 237 (2006) 267–277, https://doi.org/10.1016/j.jcat.2005.11.011.

[38] L. Huang, Q. Li, Enhanced acidity and thermal stability of mesoporous materials with post-treatment with phosphoric acid, Chem. Lett. (1999) 829–830.

[39] H.E. Van Der Bij, F. Meirer, S. Kalirai, J. Wang, B.M. Weckhuysen, Hexane cracking over steamed phosphated zeolite H-ZSM-5: Promotional effect on catalyst performance and stability, Chem. A Eur. J. 20 (2014) 16922–16932, https://doi.org/10.1002/chem.201404924.

[40] G. Caeiro, P. Magnoux, J.M. Lopes, F.R. Ribeiro, S.M.C. Menezes, A.F. Costa, H. S. Cerqueira, Stabilization effect of phosphorus on steamed H-MFI zeolites, Appl. Catal. A Gen. 314 (2006) 160–171, https://doi.org/10.1016/j.apcata.2006.08.016.

[41] A. Corma, J. Mengual, P.J. Miguel, Stabilization of ZSM-5 zeolite catalysts for steam catalytic cracking of naphtha for production of propene and ethene, Appl. Catal. A, Gen. 421–422 (2012) 121–134, https://doi.org/10.1016/j.apcata.2012.02.008.

[42] O.D. Mante, F.A. Agblevor, S.T. Oyama, R. McClung, The effect of hydrothermal treatment of FCC catalysts and ZSM-5 additives in catalytic conversion of biomass, Appl. Catal. A Gen. 445–446 (2012) 312–320, https://doi.org/10.1016/j.apcata.2012.08.039.

[43] W. Yao, J. Li, Y. Feng, W. Wang, X. Zhang, Q. Chen, S. Komarneni, Y. Wang, Thermally stable phosphorus and nickel modified ZSM-5 zeolites for catalytic co-pyrolysis of biomass and plastics, RSC Adv. 5 (2015) 1–4, https://doi.org/10.1039/C5RA02947C.

[44] I. Torre, J.M. Arandes, P. Castano, M. Azkoiti, J. Bilbao, H.I. de Lasa, Catalytic cracking of plastic pyrolysis waxes with vacuum gasoil: effect of HZSM-5 zeolite in the FCC catalyst, Int. J. Chem. React. Eng. 4 (2006).

[45] R.H. Harding, A.W. Peters, J.R.D. Nee, New developments in FCC catalyst technology, Appl. Catal. A Gen. 221 (2001) 389–396, https://doi.org/10.1016/S0926-860X(01)00814-6.

[46] H.E. van der Bij, B.M. Weckhuysen, Phosphorus promotion and poisoning in zeolite-based materials: synthesis, characterisation and catalysis, Chem. Soc. Rev. 44 (2015) 7406–7428, https://doi.org/10.1039/C5CS00109A.

[47] J.N. Louwen, L. van Eijck, C. Vogt, E.T.C. Vogt, Understanding the activation of ZSM-5 by phosphorus: localizing phosphate groups in the pores of phosphate-stabilized ZSM-5, Chem. Mater. (2020), https://doi.org/10.1021/ACS.CHEMMATER.0C03411.

[48] H.E. van der Bij, B.M. Weckhuysen, Local silico-aluminophosphate interfaces within phosphated H-ZSM-5 zeolites, Phys. Chem. Chem. Phys. 16 (2014) 9892, https://doi.org/10.1039/c3cp54791d.

[49] T.F. Degnan, G.K. Chitnis, P.H. Schipper, History of ZSM-5 fluid catalytic cracking additive development at Mobil, Microporous Mesoporous Mater. 35–36 (2000) 245–252, https://doi.org/10.1016/S1387-1811(99)00225-5.

[50] Y.J. Lee, J.M. Kim, J.W. Bae, C.H. Shin, K.W. Jun, Phosphorus induced hydrothermal stability and enhanced catalytic activity of ZSM-5 in methanol to DME conversion, Fuel 88 (2009) 1915–1921, https://doi.org/10.1016/j.fuel.2009.04.007.

[51] N. Xue, X. Chen, L. Nie, X. Guo, W. Ding, Y. Chen, M. Gu, Z. Xie, Understanding the enhancement of catalytic performance for olefin cracking: Hydrothermally stable acids in P/HZSM-5, J. Catal. 248 (2007) 20–28, https://doi.org/10.1016/j.jcat.2007.02.022.

[52] G. Zhao, J. Teng, Z. Xie, W. Jin, W. Yang, Q. Chen, Y. Tang, Effect of phosphorus on HZSM-5 catalyst for C4-olefin cracking reactions to produce propylene, J. Catal. 248 (2007) 29–37, https://doi.org/10.1016/j.jcat.2007.02.027.

[53] N. Xue, L. Nie, D. Fang, X. Guo, J. Shen, W. Ding, Y. Chen, Synergistic effects of tungsten and phosphorus on catalytic cracking of butene to propene over HZSM-5, Appl. Catal. A Gen. 352 (2009) 87–94, https://doi.org/10.1016/j.apcata.2008.09.029.

[54] A. Corma, J. Mengual, P.J. Miguel, Stabilization of ZSM-5 zeolite catalysts for steam catalytic cracking of naphtha for production of propene and ethene, Appl. Catal. A Gen. 421–422 (2012) 121–134, https://doi.org/10.1016/j.apcata.2012.02.008.

[55] Y. Xue, Thermochemical conversion of organic and plastic waste materials through pyrolysis, (2017).

[56] A. Eschenbacher, R.J. Varghese, M. SeifaliAbbas-Abadi, K.M.Van Geem, Maximizing light olefins and aromatics as high value base chemicals via single step catalytic conversion of plastic waste, Chem. Eng. J. (2021), 132087, https://doi.org/10.1016/J.CEJ.2021.132087.

[57] A. Eschenbacher, F. Goodarzi, R.J. Varghese, K. Enemark-Rasmussen, S. Kegnæs, M.S. Abbas-Abadi, K.M.Van Geem, Boron-modified mesoporous ZSM-5 for the conversion of pyrolysis vapors from LDPE and mixed polyolefins: maximizing the C 2 –C 4 olefin yield with minimal carbon footprint, ACS Sustain. Chem. Eng. 9 (2021) 14618–14630, https://doi.org/10.1021/acssuschemeng.1c06098.

[58] C.A. Emeis, Determination of integrated molar extinction coefficients for infrared absorption bands of pyridine adsorbed on solid acid catalysts, J. Catal. 141 (1993) 347–354, https://doi.org/10.1006/jcat.1993.1145.

[59] K. Schofield, The enigmatic mechanism of the flame ionization detector: its overlooked implications for fossil fuel combustion modeling, Prog. Energy Combust. Sci. 34 (2008) 330–350, https://doi.org/10.1016/j.pecs.2007.08.001.

[60] Y. Xue, P. Johnston, X. Bai, Effect of catalyst contact mode and gas atmosphere during catalytic pyrolysis of waste plastics, Energy Convers. Manag. 142 (2017) 441–451.

[61] Y. Shen, Z. Qin, S. Asahina, N. Asano, G. Zhang, S. Qian, Y. Ma, Z. Yan, X. Liu, S. Mintova, The inner heterogeneity of ZSM-5 zeolite crystals, J. Mater. Chem. A. 9 (2021) 4203–4212, https://doi.org/10.1039/d0ta11023j.

[62] R.M. Dessau, E.W. Valyocsik, N.H. Goeke, Aluminum zoning in ZSM-5 as revealed by selective silica removal, Zeolites 12 (1992) 776–779, https://doi.org/10.1016/0144-2449(92)90049-U.

[63] D. Fodor, F. Krumeich, R. Hauert, J.A.Van Bokhoven, Differences between individual ZSM-5 crystals in forming hollow single crystals and mesopores during base leaching, Chem. - A Eur. J. 21 (2015) 6272–6277, https://doi.org/10.1002/chem.201406182.

[64] D. Verboekend, S. Mitchell, M. Milina, J.C. Groen, J. Pérez-Ramírez, J. Peréz-Ramírez, J. Pérez-Ramírez, Full compositional flexibility in the preparation of mesoporous MFI zeolites by desilication, J. Phys. Chem. C 115 (2011) 14193–14203, https://doi.org/10.1021/jp201671s.

[65] H. Chen, H. Cheng, F. Zhou, K. Chen, K. Qiao, X. Lu, P. Ouyang, J. Fu, Catalytic fast pyrolysis of rice straw to aromatic compounds over hierarchical HZSM-5 produced by alkali treatment and metal-modification, J. Anal. Appl. Pyrolysis 131 (2018) 76–84, https://doi.org/10.1016/j.jaap.2018.02.009.

[66] A. Yamaguchi, D. Jin, T. Ikeda, K. Sato, N. Hiyoshi, T. Hanaoka, F. Mizukami, M. Shirai, Deactivation of ZSM-5 zeolite during catalytic steam cracking of n-hexane, Fuel Process. Technol. 126 (2014) 343–349, https://doi.org/10.1016/J.FUPROC.2014.05.013.

[67] L.H. Ong, M.M. Dömök, R. Olindo, A.C. Van Veen, J.A. Lercher, A.C. van Veen, J. A. Lercher, Dealumination of HZSM-5 via steam-treatment, Microporous Mesoporous Mater. 164 (2012) 9–20, https://doi.org/10.1016/j.micromeso.2012.07.033.

[68] A.P. Hawkins, A. Zachariou, S.F. Parker, P. Collier, N. Barrow, I.P. Silverwood, R. F. Howe, D. Lennon, Effect of steam de-alumination on the interactions of propene with H-ZSM-5 zeolites, RSC Adv. 10 (2020) 23136–23147, https://doi.org/10.1039/d0ra03871g.

[69] X. Gao, Z. Tang, H. Zhang, C. Liu, Z. Zhang, G. Lu, D. Ji, High performance phosphorus-modified ZSM-5 zeolite for butene catalytic cracking, Korean J. Chem. Eng. 27 (2010) 812–815, https://doi.org/10.1007/s11814-010-0134-6.

[70] H.E. Van Der Bij, B.M. Weckhuysen, Local silico-aluminophosphate interfaces within phosphated H-ZSM-5 zeolites, Phys. Chem. Chem. Phys. 16 (2014) 9892–9903, https://doi.org/10.1039/c3cp54791d.

[71] G.L. Woolery, G.H. Kuehl, On the nature of framework Brønsted and Lewis acid sites in ZSM-5, Zeolites 19 (1997) 288–296, https://doi.org/10.1016/S0144-2449(97)00086-9.

[72] J. Zhuang, D. Ma, G. Yang, Z. Yan, X. Liu, X. Liu, X. Han, X. Bao, P. Xie, Z. Liu, Solid-state MAS NMR studies on the hydrothermal stability of the zeolite catalysts for residual oil selective catalytic cracking, J. Catal. 228 (2004) 234–242, https://doi.org/10.1016/j.jcat.2004.08.034.

[73] K. Damodaran, J.W. Wiench, S.M. Cabral de Menezes, Y.L. Lam, J. Trebosc, J. P. Amoureux, M. Pruski, Modification of H-ZSM-5 zeolites with phosphorus. 2. Interaction between phosphorus and aluminum studied by solid-state NMR spectroscopy, Microporous Mesoporous Mater. 95 (2006) 296–305, https://doi.org/10.1016/j.micromeso.2006.05.034.

[74] H.E. Van Der Bij, L.R. Aramburo, B. Arstad, J.J. Dynes, J. Wang, B. M. Weckhuysen, Phosphatation of zeolite H-ZSM-5: A combined microscopy and spectroscopy study, ChemPhysChem 15 (2014) 283–292, https://doi.org/10.1002/cphc.201300910.

[75] G. Lischke, R. Eckelt, H.G. Jerschkewitz, B. Parlitz, E. Schreier, W. Storek, B. Zibrowius, G. Öhlmann, Spectroscopic and physicochemical characterization of P-Modified H-ZSM-5, J. Catal. 132 (1991) 229–243, https://doi.org/10.1016/0021-9517(91)90259-7.

[76] G. Seo, R. Ryoo, 31P, 27Al, and 129Xe NMR study of phosphorus-impregnated HZSM-5 zeolite catalysts, J. Catal. 124 (1990) 224–230, https://doi.org/10.1016/0021-9517(90)90117-3.

[77] T.M. Duncan, D. DOUGLASS, On the P-31 chemical-shift anisotropy in condensed phosphates, Chem. Phys. 87 (1984) 339–349.

[78] D.B. Parekh, Y.C. Rotliwala, P.A. Parikh, Synergetic pyrolysis of high density polyethylene and Jatropha and Karanj cakes: a thermogravimetric study, J. Renew. Sustain. Energy 1 (2009), 033107, https://doi.org/10.1063/1.3153904.

[79] M.P. Kothandaraman, M. Somasundaram, Non-isothermal kinetic study on copyrolysis of Juliflora and low-density polyethylene, Biomass Convers. Biorefinery. (2019), https://doi.org/10.1007/s13399-019-00559-2.

[80] S. Tsuge, Y. Sugimura, T. Nagaya, Structural characterization of polyolefins by pyrolysis-hydrogenation glass capillary gas chromatography, J. Anal. Appl. Pyrolysis 1 (1980) 221–229, https://doi.org/10.1016/0165-2370(80)80005-2.

[81] L. Sojáka, R. Kubineca, H. Jurdáková, E. Hájeková, M. Bajus, Gc-Ms of polyethylene and polypropylene thermal cracking products, Pet. Coal. 48 (2006) 1–14.

[82] I. Çit, A. Sinağ, T. Yumak, S. Uçar, Z. Misirlioğlu, M. Canel, Comparative pyrolysis of polyolefins (PP and LDPE)and PET, Polym. Bull. 64 (2010) 817–834, https://doi.org/10.1007/s00289-009-0225-x.

[83] M.T.S.P. De Amorim, C. Comel, P. Vermande, Pyrolysis of polypropylene, J. Anal. Appl. Pyrolysis 4 (1982) 73–81, https://doi.org/10.1016/0165-2370(82)80028-4.

[84] P. Kusch, Application of Pyrolysis-Gas Chromatography/Mass Spectrometry (Py-GC/MS), Elsevier Ltd, 2017, https://doi.org/10.1016/bs.coac.2016.10.003.

[85] L. Ballice, R. Reimert, Classification of volatile products from the temperature-programmed pyrolysis of polypropylene (PP), atactic-polypropylene (APP) and thermogravimetrically derived kinetics of pyrolysis, Chem. Eng. Process. 41 (2002) 289–296, https://doi.org/10.1016/S0255-2701(01)00144-1.

[86] J. Scheirs, Overv. Commer. Pyrolysis Process. Waste Plast. (2006), https://doi.org/10.1002/0470021543.ch15.

[87] S. Hafeez, E. Pallari, G. Manos, A. Constantinou, Catalytic Conversion and Chemical Recovery, Elsevier Inc,, 2018, https://doi.org/10.1016/B978-0-12-813140-4.00006-6.

[88] S. Teketel, W. Skistad, S. Benard, U. Olsbye, K.P. Lillerud, P. Beato, S. Svelle, Shape selectivity in the conversion of methanol to hydrocarbons: The catalytic performance of one-dimensional 10-ring zeolites: ZSM-22, ZSM-23, ZSM-48, and EU-1, ACS Catal. 2 (2012) 26–37, https://doi.org/10.1021/cs200517u.

[89] J. Scheirs, W. Kaminsky, Feedstock Recycl. Pyrolysis Waste Plast.: Convert. Waste Plast. into Diesel Other Fuels (2006), https://doi.org/10.1002/s1351-4180(06)71853-0.

[90] A. Akah, M. Al-Ghrami, M. Saeed, M.A.B. Siddiqui, Reactivity of naphtha fractions for light olefins production, Int. J. Ind. Chem. 8 (2017) 221–233, https://doi.org/10.1007/s40090-016-0106-8.

[91] M. del, R. Hernández, A. Gómez, Á.N. García, J. Agulló, A. Marcilla, Effect of the temperature in the nature and extension of the primary and secondary reactions in the thermal and HZSM-5 catalytic pyrolysis of HDPE, Appl. Catal. A Gen. 317 (2007) 183–194, https://doi.org/10.1016/j.apcata.2006.10.017.

[92] P.N. Sharratt, Y.H. Lin, A.A. Garforth, J. Dwyer, Investigation of the catalytic pyrolysis of high-density polyethylene over a HZSM-5 catalyst in a laboratory fluidized-bed Reactor, Ind. Eng. Chem. Res. 36 (1997) 5118–5124, https://doi.org/10.1021/ie970348b.

[93] K.M. van Geem, V.V. Galvita, G.B. Marin, Making chemicals with electricity, Sci. (80-.) 364 (2019) 734–735, https://doi.org/10.1126/science.aax5179.

[94] M. Shekarchian, F. Zarifi, M. Moghavvemi, F. Motasemi, T.M.I. Mahlia, Energy, exergy, environmental and economic analysis of industrial fired heaters based on heat recovery and preheating techniques, Energy Convers. Manag 71 (2013) 51–61, https://doi.org/10.1016/j.enconman.2013.03.008.

[95] A.M. Bassily, G.M. Colver, Modelling and performance analysis of an electric heater, Int. J. Energy Res. 28 (2004) 1269–1291, https://doi.org/10.1002/er.1029.

[96] G. Wernet, C. Bauer, B. Steubing, J. Reinhard, E. Moreno-Ruiz, B. Weidema, The ecoinvent database version 3 (part I): overview and methodology, Int. J. Life Cycle Assess. 21 (2016) 1218–1230, https://doi.org/10.1007/s11367-016-1087-8.

[97] E. Delikonstantis, E. Igos, S.A. Theofanidis, E. Benetto, G.B. Marin, K. Van Geem, G.D. Stefanidis, An assessment of electrified methanol production from an environmental perspective, Green. Chem. 23 (2021) 7243–7258, https://doi.org/10.1039/d1gc01730f.

[98] E. Delikonstantis, E. Igos, M. Augustinus, E. Benetto, G.D. Stefanidis, Life cycle assessment of plasma-assisted ethylene production from rich-in-methane gas streams, Sustain, Energy Fuels 4 (2020) 1351–1362, https://doi.org/10.1039/c9se00736a.

[99] T. Ren, M.K. Patel, K. Blok, Steam cracking and methane to olefins: energy use, CO_2 emissions and production costs, Energy 33 (2008) 817–833, https://doi.org/10.1016/j.energy.2008.01.002.

[100] P.J. Donaj, W. Kaminsky, F. Buzeto, W. Yang, Pyrolysis of polyolefins for increasing the yield of monomers' recovery, Waste Manag 32 (2012) 840–846, https://doi.org/10.1016/j.wasman.2011.10.009.

[101] M. Artetxe, G. Lopez, G. Elordi, M. Amutio, J. Bilbao, M. Olazar, Production of light olefins from polyethylene in a two-step process: Pyrolysis in a conical spouted bed and downstream high-temperature thermal cracking, Ind. Eng. Chem. Res. 51 (2012) 13915–13923, https://doi.org/10.1021/ie300178e.

[102] J.A. Conesa, R. Font, A. Marcialla, A.N. Garcia, Pyrolysis of polyethylene in a fluidised bed reactor, CHISA 2008 - 18th Int. Congr. Chem. Process Eng. (2008) 1238–1246.

[103] M. Della Zassa, M. Favero, P. Canu, Two-steps selective thermal depolymerization of polyethylene. 1: feasibility and effect of devolatilization heating policy, J. Anal. Appl. Pyrolysis 87 (2010) 248–255, https://doi.org/10.1016/j.jaap.2010.01.003.

[104] M. Del Remedio Hernández, Á.N. García, A. Marcilla, Study of the gases obtained in thermal and catalytic flash pyrolysis of HDPE in a fluidized bed reactor, J. Anal. Appl. Pyrolysis 73 (2005) 314–322, https://doi.org/10.1016/j.jaap.2005.03.001.

[105] B.J. Milne, L.A. Behie, F. Berruti, Recycling of waste plastics by ultrapyrolysis using an internally circulating fluidized bed reactor, J. Anal. Appl. Pyrolysis 51 (1999) 157–166, https://doi.org/10.1016/S0165-2370(99)00014-5.

[106] R.W.J. Westerhout, J. Waanders, J.A.M. Kuipers, W.P.M.Van Swaaij, Development of a continuous rotating cone reactor pilot plant for the pyrolysis of polyethene and polypropene, Ind. Eng. Chem. Res. 37 (1998) 2316–2322, https://doi.org/10.1021/ie970703y.

[107] A. Corma, E. Corresa, Y. Mathieu, L. Sauvanaud, S. Al-Bogami, M.S. Al-Ghrami, A. Bourane, Crude oil to chemicals: Light olefins from crude oil, Catal. Sci. Technol. 7 (2017) 12–46, https://doi.org/10.1039/c6cy01886f.

[108] N. Nikolopoulos, R.G. Geitenbeek, G.T. Whiting, B.M. Weckhuysen, Unravelling the effect of impurities on the methanol-to-olefins process in waste-derived zeolites ZSM-5, J. Catal. 396 (2021) 136–147, https://doi.org/10.1016/j.jcat.2021.02.015.